1   **Zika virus-specific IgM elicited during pregnancy exhibits ultrapotent neutralization**

2   Tulika Singh[1,2], Kwan-Ki Hwang[1,§], Andrew S. Miller[3], Rebecca L. Jones[1], Cesar A. Lopez[4],

3   Camila Giuberti[5], Morgan A. Gladden[1], Itzayana Miller[1,6], Helen S. Webster[1], Joshua A.

4   Eudailey[1,6], Kan Luo[1], Tarra Von Holle[1], Robert J. Edwards[1], Sarah Valencia[1], Katherine E.

5   Burgomaster[7], Summer Zhang[8], Jesse F. Mangold[1,†], Joshua J. Tu[1], Maria Dennis[1], S. Munir

6   Alam[1], Lakshmanane Premkumar[4], Reynaldo Dietze[5,9], Theodore C. Pierson[7], Eng Eong Ooi[8],

7   Helen M. Lazear[4], Richard J. Kuhn[3], Sallie R. Permar[1,6]*, Mattia Bonsignori[1,10]*

8

9   [1]Duke Human Vaccine Institute, Duke University School of Medicine, Durham, NC 27710, USA

10   [2]Division of Infectious Diseases and Vaccinology, School of Public Health, University of California,
11   Berkeley, Berkeley, CA 94709, USA.

12   [3]Department of Biological Sciences, Purdue Institute of Inflammation, Immunology, and Infectious
13   Disease, Purdue University, West Lafayette, IN 47907, USA

14   [4]Department of Microbiology and Immunology, University of North Carolina at Chapel Hill, Chapel
15   Hill, NC 27599, USA

16   [5]Núcleo de Doenças Infecciosas, Universidade Federal do Espírito Santo, Vitoria, Espírito Santo
17   29075-910, Brazil

18   [6]Department of Pediatrics, Weill Cornell Medicine, New York City, NY 10065, USA

19   [7]Viral Pathogenesis Section, Laboratory of Viral Diseases, National Institute of Allergy and Infectious
20   Diseases, National Institutes of Health, Bethesda, MD 20892 USA.

21   [8]Duke-National University of Singapore Medical School, 169857, Singapore

22   [9]Global Health & Tropical Medicine, Instituto de Higiene e Medicina Tropical, Universidade Nova
23   de Lisboa, Lisbon 1349-008, Portugal

24   [10]Translational Immunobiology Unit, Laboratory of Infectious Diseases, National Institute of
25   Allergy and Infectious Diseases, National Institutes of Health, Bethesda, MD 20892, USA

26   § Current address: 124 Cosgrove Ave, Chapel Hill, NC 27514, USA

27   † Current address: Department of Microbiology, Icahn School of Medicine, New York City, NY
28   10029-6574, USA

29

30   *Correspondence: sap4017@med.cornell.edu (S.R.P.), mattia.bonsignori@nih.gov (M.B.)

31

Key points

1. Plasma IgM contributes to early ZIKV neutralization during pregnancy

2. Ultrapotent neutralization by pentameric DH1017.IgM mAb depends on isotype

3. DH1017.IgM can engage all binding sites concurrently through different angles of approach

4. DH1017.IgM protects mice against lethal ZIKV challenge

Summary

Congenital Zika virus (ZIKV) infection results in neurodevelopmental deficits in up to 14% of infants born to ZIKV-infected mothers. Neutralizing antibodies are a critical component of protective immunity. Here, we demonstrate that plasma IgM responses contribute to ZIKV immunity in pregnancy, mediating neutralization up to three months post symptoms. From a ZIKV-infected pregnant woman, we established a B cell line secreting a pentameric ZIKV-specific IgM (DH1017.IgM) that exhibited ultrapotent ZIKV neutralization dependent on the IgM isotype. DH1017.IgM targets a novel envelope dimer epitope within Domain II. The arrangement of this epitope on the virion is compatible with concurrent engagement of all ten antigen-binding sites of DH1017.IgM, a solution not achievable by IgG antibodies. DH1017.IgM protected against lethal ZIKV challenge in mice. Our findings identify a unique role of antibodies of the IgM isotype in protection against ZIKV and posit DH1017.IgM as a safe and effective candidate immunoprophylactic, particularly during pregnancy.

Introduction

Zika virus (ZIKV) emergence in the Americas revealed it to be congenitally transmitted, causing microcephaly and other birth defects in up to 14% of infants born to ZIKV-infected pregnancies (Reynolds et al., 2017). Even infants born seemingly healthy following maternal ZIKV infection may develop neurodevelopmental defects years later (Nielsen-Saines et al., 2019). As ZIKV mostly results in mild febrile disease in healthy adults, its greatest disease burden arises through infections in pregnancy. In the 2015-2016 epidemic, ZIKV re-emergence in a susceptible population led to 11,000 cases of microcephaly in Brazil alone (Campos et al., 2018). There is no licensed vaccine for ZIKV, and the vaccine development and testing pipeline has stalled due to limited ZIKV circulation (Morabito and Graham, 2017).

Protective immunity in pregnancy could prevent ZIKV infection, congenital transmission, and lifelong congenital Zika syndrome sequelae. Neutralizing antibodies (nAbs) have been shown to be a critical aspect of protective immune responses against ZIKV and other flavivirus infections (Abbink et al., 2016; Hombach et al., 2005; Katzelnick et al., 2017; Kreil et al., 1997; Kwek et al., 2018; Larocca et al., 2016; Mason et al., 1973; Richner et al., 2017), yet nAb studies have largely focused on IgG antibodies. However, flavivirus infections are also characterized by virus-specific and prolonged IgM responses. IgM are pentameric molecules with 5-times as many potential antigen binding sites compared to IgG. Conventionally, IgM are thought of as early, short-lived, and low-affinity antibodies that are not somatically matured and thus unable to confer potent viral neutralization. Yet, early neutralizing IgM responses have been identified for other flaviviruses such as West Nile virus and yellow fever virus (Diamond et al., 2003; Gasser et al., 2020; Monath, 1971; Wec et al., 2020). A common feature is that these viruses present dense and repetitive structures on their surface, which may favor avid multivalent interactions with B cell receptors and influence the functional antibody profile via B cell stimulation and clonal selection. Interestingly, long-lasting ZIKV-reactive IgM responses have recently been independently identified in two distinct populations (Griffin et al., 2019; Stone et al., 2020). The presence of ZIKV-specific IgM lasting up to multiple years, when the typical half-life of IgM is 5 days, suggests that ZIKV-reactive IgM expressing B cells are specifically activated and expanded upon ZIKV infection (Lobo et al., 2004). While neutralizing activity is primarily attributed to IgG isotype antibodies, IgM may have an underappreciated role in ZIKV immunity.

The role of ZIKV IgM and IgM-producing B cells is especially understudied in pregnancy, a period of differential immunomodulation where ZIKV infections lead to their greatest disease burden. Early in pregnancy B cells are stimulated to produce IL-10, and subsequently B cell lymphopoiesis is suppressed, which promotes survival of mature B cells and decreases circulating naive B cell frequency (Christiansen et al., 1976; Lima et al., 2016; Nguyen et al., 2013). Retention of the IgM isotype diminishes as B cells differentiate from naïve to memory and antibody-secreting cells, which shapes B cell clonal selection in response to infection and long-lasting protective immunity (King et al., 2021). These factors may impact the magnitude and quality of ZIKV-specific IgM and IgG immunity in pregnancy.

In this study, we sought to define the kinetics and role of IgM in the control of ZIKV infection during pregnancy. We evaluated the contribution of plasma IgM to ZIKV neutralization in pregnant

4

91 women over time and demonstrated that, in pregnancy, plasma IgM contributes to ZIKV
92 neutralization primarily within the first 3 months of infection, regardless of prior exposure to other
93 flaviviruses. We probed the B cell repertoire from peripheral blood of mothers with primary and
94 secondary ZIKV infections and established 9 ZIKV-binding B lymphoblastoid cell lines (B-LCL).
95 One of them produced an IgM antibody, DH1017.IgM, in its native pentameric conformation.
96 DH1017.IgM was somatically mutated, did not cross-react with other flaviviruses, and displayed
97 ultrapotent ZIKV neutralization that depended on its isotype. Structural studies identified a mode
98 of antigen recognition on the ZIKV virion surface compatible with the concurrent engagement of
99 all ten antigen-binding sites, a solution that is not available to antibodies of the IgG isotype, which
100 have only two antigen-binding sites. The ultrapotent activity and protection mediated by
101 DH1017.IgM in mice suggest that DH1017.IgM is a candidate for anti-ZIKV immunoprophylaxis.

102

103 **Results**

104 **IgM contributes to plasma ZIKV neutralization during early phases of infection in pregnant**
105 **women.**

106 We previously described a cohort of pregnant women from the 2015-2016 ZIKV outbreak in Brazil
107 who presented with ZIKV-like symptoms of fever and/or rash in pregnancy and were serologically
108 confirmed for ZIKV infection (Singh et al., 2019). Serologic evidence of prior exposure to DENV
109 was demonstrated in most ZIKV-infected mothers in the cohort, and termed secondary ZIKV
110 (Singh et al., 2019). Both primary (P24 and P54) and secondary (P14, P15, P17, P19, P23, P50,
111 P56 and P73) ZIKV infection cases were included in this study. Among them, eight women were
112 diagnosed during acute infection by serum PCR and two were identified as ZIKV-exposed based
113 on ZIKV and DENV 1-4 neutralization titers (Singh et al., 2019). From 9 subjects, pregnancy and
114 delivery plasma samples were available between 8- and 406-days post-symptoms (DPS). From
115 1 subject (P73), multiple longitudinal samples were collected between 8-406 DPS. Subject P73
116 developed prolonged viremia (up to 42 DPS), while all other subjects were viremic only up to their
117 first visit (Singh et al., 2019). All subjects had high levels of ZIKV-neutralizing plasma antibodies
118 at delivery (median $FRNT_{50}$ = 4566; range: 650–14,959) (Singh et al., 2019).

119 To evaluate the contribution of plasma IgM to ZIKV neutralization during pregnancy, we measured
120 total IgM and IgG concentrations, ZIKV binding IgG, and ZIKV neutralization of paired samples
121 after mock and IgM depletion (**Table S1**). Subject P73 displayed the highest IgM-mediated ZIKV
122 plasma neutralization, which started modestly at 8 DPS (7%), then rapidly peaked to 78% at 14
123 DPS ranging from 3% to 52% up to 112 DPS following a multimodal distribution and waned
124 thereafter to undetectable levels. (**Figure 1**). An important contribution of IgM to plasma ZIKV
125 neutralization was confirmed across all the samples collected between 14 and 100 DPS from
126 each of the other subjects (range: 17-49%), regardless of serostatus (i.e., primary or secondary
127 ZIKV infection). IgM plasma contribution was minimal to null in samples collected during late
128 infection (range: 0-4%), except for subject P23, who displayed 28% of IgM-mediated ZIKV
129 neutralization at 209 DPS. Overall, 90% (9/10) of plasma samples collected within 3 months of
130 symptomatic infection from 4 mothers demonstrated >10% IgM-attributable ZIKV neutralization,
131 but only 18% (2/11) of samples from beyond 3 months demonstrated this response (**Figure 1**).

5

Isolation of ZIKV-specific, ultrapotent neutralizing mAb DH1017.IgM.

We next probed the B cell compartment of subject P73 at 28 and 71 DPS to identify B cells producing ZIKV-neutralizing IgM. We also selected four ZIKV-infected pregnant women from the same cohort (Singh et al., 2019), including one woman with primary ZIKV infection (P54: 29 and 77 DPS) and three women with secondary ZIKV infection (P34 at 162 DPS, P56 at 19 DPS, and P73 at 28 and 71 DPS) for a comparative analysis of the ZIKV-specific B cell repertoire. We enriched for ZIKV-reactive B cells by sorting either unfractionated or memory B cells (MBCs) using a fluorescent ZIKV virion as bait and cultured cells at limiting dilution to derive human B-LCL through EBV transformation as described (Bonsignori et al., 2011, 2018).

Across subjects, ZIKV-reactive B cells constituted 0.6-1.7% of the circulating unfractionated B cell pool (**Figure S1A**). Regardless of serostatus and time of sample collection relative to symptoms onset, the frequency of ZIKV-reactive MBCs out of total MBCs was uniformly higher than the ZIKV-reactive B cells out of the total unfractionated B cell pool (0.7-2.6% vs 0.6-1.7%; p<0.03, paired t-test) (**Figure S1A**). On average, ZIKV-reactive memory B cells comprised 52% of total ZIKV-reactive B cells with higher frequencies observed in secondary infections (P73, P56, P34) than in the primary ZIKV infection case (P54) (46-69% vs 34%; **Figure S1B**), compatible with a re-engagement of pre-existing cross-reactive memory B cells in secondary infection.

In vitro B cell stimulation across all 4 subjects yielded a total of 97 Ig-secreting culture supernatants, of which 37 were from unfractionated B cells and 60 from memory B cells. Among unfractionated cultures, 13 cultures contained both IgG and IgM, whereas all cultures from memory B cells were of a single Ig isotype. Ig concentrations ranged from 3 to >3000 ng/ml with a geometric mean of 146 ng/ml. Overall, 49 of 97 (50.5%) Ig-secreting culture supernatants confirmed ZIKV reactivity: 17 (15 IgG and 2 IgM) from unfractionated B cells and 32 (all IgG) from memory B cell cultures (**Figure S1C**). From ZIKV-reactive Ig-secreting cultures, we established 9 B-LCL, 8 of which produced IgG monoclonal antibodies (mAbs) and one, termed DH1017.IgM, produced an IgM mAb.

Analysis of the Ig V(D)J rearrangement immunogenetics demonstrated that none of the B-LCLs were clonally related (**Table 1**). Diverse heavy chain variable gene segments were used and paired with either κ or λ light chains (V_L), without V_H/V_L pairing preferences. CDRH3 lengths ranged between 12 and 22 amino acids (median: 15 amino acids). Overall, V_H and V_L somatic hypermutation (SHM) frequency ranged from 3.1% to 10.8%, and 1.5% to 8.0%, respectively (**Table 1**). The V_H SHM frequency of sequences obtained from unfractionated B cells and memory B cells was statistically similar (p>0.05, Kolmogorov-Smirnov test). DH1017.IgM used the V_H4-31 gene segment paired with V_λ 1-51 and had a 15 amino acid-long CDRH3 (**Table 1**). While the B cell that expressed DH1017.IgM was isolated from unfractionated B cells and we could not determine its origin from the naïve or memory B cell compartment, the SHM frequency in the DH1017.IgM V(D)J rearrangements were within the range of other IgG mAbs that we isolated (3.8% for the heavy chain and 3.4% for the light chain) with 7 nucleotide mutations in the V_H and 9 in the V_L. All but two of these nucleotide changes were substitution mutations. Nine of the 16 nucleotide substitutions (56%) occurred in canonical activation-induced cytidine deaminase (AID)

172 hotspot motifs with high mutability rates (Yaari et al., 2013). The remaining 7 substitutions
173 occurred in neutral or cold-spot motifs (**Table S2**).

174 MAbs were produced and purified from the 9 B-LCLs for functional characterization. In a native
175 gel, mAb DH1017.IgM yielded two bands at ~970 kDa and ~1048 KDa (**Figure 2A**), which is
176 compatible with pentameric and hexameric IgM isoforms (Keyt et al., 2020; Wiersma et al., 1998).
177 Negative stain electron microscopy class average analysis supported the presence of both
178 pentameric and hexameric isoforms, with hexamers representing 18% and pentamers
179 representing 73% of all observed images (**Figure 2A**).

180 All purified mAbs confirmed binding to ZIKV. While 126-1-D11.IgG bound weakly even at high
181 concentrations (LogAUC = 2.0), all other mAbs bound with LogAUC ranging from 2.7 to 5.9, with
182 the strongest ZIKV-binding mAb being DH1017.IgM (**Figure 2B**). Since plasma antibody
183 displayed substantial cross-reactivity with DENV in all subjects except primary infection subject
184 P54 (**Figure S2A**), we determined cross-reactivity of the nine mAbs with DENV 1-4 strains. Based
185 on their binding profile, the mAbs segregated into two clusters (**Figure 2C**). Cluster I comprised
186 mAbs 123-3-G2.IgG, 124-4-C8.IgG, 124-1-C2.IgG, and 124-2-G3.IgG that bound to one or more
187 DENV 1-4 strains better than to ZIKV. These mAbs were isolated from memory B cells of mothers
188 with secondary ZIKV-infection (P73 and P56), which parallels the plasma cross-reactivity profile
189 and further implies re-engagement of pre-existing DENV-reactive memory B cells. Conversely,
190 cluster II mAbs bound more strongly to ZIKV than to DENV, for which cross-reactivity was either
191 at or below limit of detection, which suggests that these mAbs may constitute a *de novo* immune
192 response to ZIKV. Notably, DH1017.IgM did not cross-react with or neutralize any of the four
193 DENV serotypes (**Figure 2C** and **Figure S2B**).

194 Five of the nine ZIKV-specific mAbs mediated neutralization of the ZIKV PRVABC59 strain
195 (**Figure 2D**). Mab 124-4-C8.IgG neutralized weakly with $FRNT_{50}$ >10µM. Mabs 119-1-D7.IgG,
196 119-5-C5.IgG and 119-4-D6.IgG neutralized with $FRNT_{50}$= 5.8 nM, 9.2 nM and 9.7 nM,
197 respectively. Remarkably, DH1017.IgM neutralized ZIKV with ~500- to 1000-fold higher potency
198 ($FRNT_{50}$=12 pM) (**Figure 2D**). DH1017.IgM neutralization of the ZIKV PRVABC59 strain was
199 repeated multiple times (n=10) and potent neutralization was independently confirmed by multiple
200 operators (geometric mean [GM] $FRNT_{50}$: 12 pM; range: 4-31 pM). DH1017.IgM also neutralized
201 the ZIKV H/PF/2013 strain with comparable potency (GM $FRNT_{50}$: 14 pM; range: 8-26 pM) (**Figure
202 S2C**). We compared DH1017.IgM potency with a panel of well characterized ZIKV-neutralizing
203 IgG mAbs: EDE1 C8, EDE1 C10, ZIKV-893, rZIKV-195, G9E, ZV-2, ZIKV-752, ZKA190, and
204 HuZV-67 (Collins et al., 2019; Gilchuk et al., 2020; Hasan et al., 2017a; Long et al., 2019;
205 Rouvinski et al., 2015; Sapparapu et al., 2016; Wang et al., 2017; Zhao et al., 2016). In this side-
206 by-side comparison, DH1017.IgM neutralized more potently than all other IgG ZIKV neutralizing
207 mAbs in the panel ($FRNT_{50}$ range: 95 pM – 15.5 nM) (**Figure 2E**). Neutralizing antibodies of the
208 IgG isotype with IC_{50} < 10ng/ml, i.e. 66.7pM, are defined as ultrapotent (Smith et al., 2015). Hence,
209 DH1017.IgM meets the definition of ultrapotent ZIKV-neutralizing antibody.

210

211

Impact of isotype on DH1017.IgM functions.

We recombinantly produced the Fab and IgG1 isoforms (DH1017.Fab and DH1017.IgG) and measured binding to ZIKV H/PF/2013 envelope (E) protein monomer and dimer. DH1017.IgM bound more potently than DH1017.IgG and DH1017.Fab to ZIKV E monomer (EC_{50} = 202 pM, 463 pM and 1.24 nM, respectively) (**Figure 3A**). The difference in binding potency among the different isotypes was more profound for the ZIKV E dimer: DH1017.IgM EC_{50} = 91 pM, DH1017.IgG EC_{50} = 929 pM, and DH1017.Fab EC_{50} = 25.1 nM (**Figure 3B**). To test the contribution of the Fc region of DH1017.IgM to its increased level of binding, we compared the DH1017.IgM and DH1017.IgG binding kinetics to ZIKV E dimer using a BLI format with immobilized mAb. Under these conditions, DH1017.IgM and DH1017.IgG displayed similar dissociation kinetic (k_{off} = 1.03 and 0.91 s^{-1}x10^{-2}, respectively) and affinity (K_d = 106 and 123 nM, respectively). This suggests that the μ-chain Fc of DH1017.IgM does not contribute towards its affinity for E protein.

We then assessed the ability of DH1017.IgM, DH1017.IgG and DH1017.Fab to bind to whole Zika PRVABC59 virion. DH1017.Fab only interacted weakly with ZIKV (EC_{50} >2mM) whereas DH1017.IgG bound strongly (EC_{50} = 112 pM), and DH1017.IgM bound 5-fold more potently than DH1017.IgG (EC_{50} = 22 pM) (**Figure 3C**). Remarkably, the functional difference between DH1017.IgM, DH1017.IgG and DH1017.Fab was even greater for ZIKV neutralization. DH1017.IgM neutralization potency ($FRNT_{50}$ = 9 pM) was >40-fold higher than DH1017.IgG ($FRNT_{50}$ = 366 pM; **Figure 3D**), whereas DH1017.Fab yielded a shallow neutralization curve ($FRNT_{50}$ = 93 nM) with 10,000-fold worse potency than DH1017.IgM (**Figure 3D**). These data demonstrate that DH1017.IgM increased binding and ultrapotent neutralization depended on the IgM isotype.

Since antibody-mediated complement deposition can reduce the amount of mAb required to neutralize virus, we tested the effect of complement from normal human serum (NHS) on DH1017.IgG and DH1017.IgM neutralizing activities. Exogenous human complement from NHS enhanced ZIKV neutralization potency of both mAbs in a dose-dependent manner (**Figure 3E**). At all doses of NHS tested (5-25% v/v), DH1017.IgM retained more potent neutralizing activity compared to DH1017.IgG. The largest improvement in neutralization potency was observed in the 25% NHS condition with 4.3-fold and 3.7-fold increase in potency for DH1017.IgM and DH1017.IgG, respectively (**Figure 3E**). These data demonstrate that neutralization potency of the DH1017 mAb in its IgG and IgM isoforms is enhanced in presence of complement.

Sub-neutralizing concentrations of flavivirus neutralizing IgG can mediate antibody-dependent enhancement (ADE) of viral infection through interactions of immune complexes with plasma membrane-anchored FcγR, particularly on monocytes (Chan et al., 2015; Halstead, 1988; Halstead and O'Rourke, 1977). DH1017.IgG mediated ADE in both K562 and THP-1 cells whereas DH1017.IgM did not (**Figures 3F, G**). DH1017.IgM also did not mediate ADE in THP-1.2S cells, a subclone of THP-1 cells with increased sensitivity to ADE (Chan et al., 2014) (**Figure 3H**). Similarly, DH1017.IgM did not mediate ADE in primary monocytes (**Figure S3A**). Finally, to further characterize the safety profile of DH1017.IgM, DH1017.IgG and DH1017.Fab, we measured binding to nine autoantigens associated with autoimmune diseases. All isotypes tested

8

253 negative for all antigens (**Figure S3B**). Further, they did not demonstrate intracellular
254 immunofluorescent staining of Hep-2 cells (**Figure S3C**).

255

256 **Structural characterization of the epitope of the DH1017 clone on the Zika virion**

257 Using cryo-electron microscopy (cryo-EM) and single particle reconstruction, we identified a set
258 of 4104 ZIKV H/PF/2013 particles bound with DH1017.Fab and generated a cryo-EM density
259 map. A surface shaded view of the virus-Fab complex is shown in **Figure 4A** and demonstrates
260 the sites of Fab binding to the surface of the particle. The cryo-EM density map resolution is 5.3
261 Å as determined from the Fourier Shell Correlation co-efficient 0.143 (**Figure S4A**).The C_α
262 backbone of the E glycoprotein ectodomains from the ZIKV asymmetric unit (PDB 6CO8; Sevvana
263 et al., 2018) is composed of three E monomers, chains A, C, and E (**Figure 4B**). Their position
264 in the density map is shown in **Figure S4B**. In this asymmetric unit, Chain A lies alongside the
265 antiparallel homodimer formed by chains C and E (**Figure 4B**). The fitted asymmetric unit is
266 repeated 60 times within the density map demonstrating icosahedral symmetry like previous Zika
267 virus structures (Sevvana et al., 2018; Sirohi et al., 2016).

268 The C_α backbone of the homology model of the DH1017.Fab was fit into the cryo-EM density map
269 (**Figure S4B**). It shows that the DH1017 variable domain interacts primarily with DII of all three E
270 monomers in the asymmetric unit, and at the interface of DII and DI on chains A and C (**Figure
271 4B, S4B**). The DH1017.Fab epitope footprint was defined by residues of the E ectodomain
272 glycoprotein on the surface of the virus within 6 Å from the C_α backbone of the DH1017 variable
273 domain structure (**Table S3, Figure 4B, C, D**). The DH1017.Fab paratope footprint was defined
274 by Fab residues within 6 Å from the C_α backbone of the E ectodomain glycoprotein of the virus
275 surface and included all three heavy chain CDRs and FRH3 (**Table S3**).

276 There are two 2-fold axes of symmetry on the virus surface: the icosahedral 2-fold (i2f) axis
277 delineates symmetry at the juncture of two antiparallel asymmetric units on the repetitive virion
278 surface between A and A', whereas the quasi 2-fold (q2f) axis describes symmetry within the
279 antiparallel E dimer between chains C and E (**Figure 4C**). Each asymmetric unit contains two
280 epitope footprints, at the i2f and q2f symmetry axes, respectively (**Figure 4C**). At the i2f axis one
281 half of the epitope footprint is located on chain A' and the other half of on chain A (**Figure 4C**),
282 whereas at the q2f axis, most epitope residues are on chain C, with some on chain E. (**Figure
283 4C, S4B**). At the i2f axis, one bound Fab will exclude the other i2f site related by two-fold
284 symmetry from being bound. Whereas, at the q2f axis, the position on chain C and E is fully
285 occupied. The result is an occupancy of 1.5 Fab per asymmetric unit.

286 Cryo-EM density data at the q2f axis identified as the Fab constant and variable domains occupied
287 a single position (**Figure 4A**). However, two distinct positions of Fab constant domain densities
288 could be identified at the i2f axis (**Figure 4A, S4B**). Hence, at the i2f axis the epitope can be
289 approached from two angles but at the q2f it is only approached at one angle. At the i2f axis, only
290 one apparent position for variable domain density was identified. It is most likely an average of
291 two distinct variable domains bound to the virus surface at different constant domain angles
292 (**Figure S4B**).

293   A top-down view of the virus particle shows that Fab densities at the q2f and i2f axes form a ring
294   around the 5-fold axis of symmetry (i5f) with the constant domains pointing toward the i5f axis
295   (**Figure S4C**). Computational modeling of the DH1017.IgM pentamer (PDB 2CRJ) above the
296   surface of the virion suggests the Fc domain can be centered and positioned above the i5f axis
297   with the Cμ3 ends above the constant domains of the Fabs (**Figure 5A**). The IgM Cμ2 domains
298   are flexible and can bend up to 90 degrees relative to the planar Cμ4-Cμ3-J portion, facilitating a
299   bent, umbrella-like, IgM conformation (Keyt et al., 2020; Murphy et al., 2012; Sharp et al., 2019).
300   The flexibility at Cμ2 domain suggests it is possible the arms of the DH1017.IgM pentamer can
301   bend toward the surface of the virus and each arm can contact the epitopes at q2f and i2f of
302   neighboring asymmetric units (**Figure 5A**). Such arrangement of the epitopes on the virion
303   surface may allow Fab pairs of a pentamer arm to contact epitope pairs on the virus surface either
304   at an i2f and q2f axes between neighboring asymmetric units or at the i2f and q2f axes within the
305   same asymmetric unit simultaneously, allowing DH1017.IgM a decavalent mode of epitope
306   recognition.

307   In the umbrella-like conformation, a theoretical maximum of three pentameric IgM can bind
308   concurrently to the same virion, occupying 30 of the 90 epitopes present on the virion surface
309   (**Figure 5B**). In this bent conformation, the IgM pentamer can contact five epitope pairs compared
310   to a single epitope pair for the recombinant DH1017.IgG due to the decavalent versus bivalent
311   mode of antigen recognition. Alternatively, the less bent and planar pentamer conformations may
312   bind one or more pairs of epitopes on one virus particle and bind one or more pairs of epitopes
313   on a second virus particle (**Figure 5C**). This mode of binding effectively cross-links multiple virus
314   particles into aggregates. Simultaneous engagement of five E dimers at the 5-fold axis of viral
315   symmetry demonstrates a novel mechanism of IgM-mediated neutralization of ZIKV that is not
316   available to an IgG molecule and may contribute to the dramatically enhanced IgM potency
317   compared to the IgG.

318

DH1017.IgM protects against lethal ZIKV challenge in a mouse model.

320   Finally, we sought to evaluate whether DH1017.IgM could protect against ZIKV infection in mice.
321   We administered 100μg of DH1017.IgM or a non-ZIKV binding human IgM to *Ifnar1*$^{-/-}$ mice 1 day
322   prior and 1 day following infection with 1000 FFU of ZIKV H/PF/2013 and measured viremia and
323   lethality. We found that DH1017.IgM conferred protection from lethal challenge in all mice and
324   controlled viremia to the limit of detection (3.2-3.6 Log$_{10}$ viral copies/mL) in comparison to mice
325   receiving control IgM (6.3-6.9 Log$_{10}$ viral copies/mL). In contrast, all mice in the control IgM group
326   succumbed to infection (**Figure 6A, B**). Human IgM was maintained *in vivo* at detectable levels
327   up to 4 days post challenge in both groups, or 3 days after the last administration (**Figure 6C**).
328   Thus, administration of ultrapotent DH1017.IgM protects against ZIKV disease in mice.

329

Discussion

331   In this study, we evaluated the contribution of plasma IgM responses to ZIKV neutralization in
332   pregnancy, defined the frequency of ZIKV-specific B cells isolated from peripheral blood, and

333   isolated a ZIKV-specific IgM monoclonal antibody, DH1017.IgM, in its native multimeric form.
334   Unlike previous plasma-depleted and whole plasma investigation of IgM, the isolation of a human
335   IgM mAb in its native multimeric conformation enabled direct characterization of the impact of the
336   IgM isotype on antibody function against ZIKV. DH1017.IgM did not cross-react with DENV 1-4
337   and mediated ultrapotent ZIKV neutralization. DH1017.IgM ultrapotency depended on its isotype,
338   as it neutralized >40-fold more potently than when expressed as an IgG. We mapped the footprint
339   of its discontinuous epitope within the asymmetric unit and predicted a mode of antigen
340   recognition compatible with the concurrent engagement of all the ten antigen-binding sites present
341   on the IgM pentamer, a solution not available to smaller IgG molecules with only two antigen-
342   binding sites. These findings identify a unique functional niche of IgM antibodies in protection
343   against ZIKV. Finally, we demonstrated in a murine model that DH1017.IgM protects from ZIKV
344   challenge.

345   The humoral response to ZIKV infection, like other flaviviruses, is characterized by the
346   development of persistent IgM serum antibodies (Gibney et al., 2012; Griffin et al., 2019; Monath,
347   1971; Stone et al., 2020). Recent studies have demonstrated that persisting ZIKV-specific serum
348   IgM antibodies predominantly contribute to ZIKV neutralization (Calvert et al., 2021; Malafa et al.,
349   2020). ZIKV infections during pregnancy are of particular concern due to the risk of congenital
350   transmission to the fetus and subsequent burden of disease in children. Pregnancy is
351   characterized by physiological alterations of the immune system but the characteristics of the
352   ZIKV-specific IgM response in pregnant women remained unstudied. In our cohort of pregnant
353   women, circulating IgM antibodies contributed to ZIKV neutralization primarily within the first 3
354   months of infection and as a minor contributor up to 209 DPS, which aligns with a previous report
355   of ZIKV-specific IgM nAb dynamics outside pregnancy (Calvert et al., 2021). The temporal
356   association (10-14 days post infection) between clearance of ZIKV infection in most individuals
357   (Lessler et al., 2016; Paz-Bailey et al., 2018) and the early peak of serum IgM which precedes
358   peak IgG responses (Ravichandran et al., 2019; Tonnerre et al., 2020) suggests that early IgM
359   neutralizing responses may play an important role in early control of infection. Our data extend
360   such temporal association in the setting of pregnancy.

361   We note that subject P73, from whom we isolated DH1017.IgM at day 71 DPS, developed a
362   prolonged viremia lasting 42 days despite an early robust peak in plasma IgM neutralization.
363   However, while viremia outlasted the first plasma IgM neutralization peak in this subject, high
364   levels of IgM ZIKV neutralization persisted up to 71 DPS, 30 days after viremia control. The
365   relationship between prolonged viremia and robustness of plasma IgM should be further
366   investigated.

367   While the role of serum IgM in flavivirus infection is actively being studied, ZIKV-specific IgM
368   monoclonal antibodies have not been characterized, hindering our understanding of the
369   mechanisms of action of this isotype against ZIKV. From subject P73, we derived a fully human
370   IgM-expressing B-LCL secreting the ZIKV-specific ultrapotent DH1017.IgM nAb in its native
371   multimeric conformation. While subject P73 had a prior exposure to DENV, DH1017.IgM did not
372   bind to DENV and was therefore not part of a recall response from pre-existing DENV immunity.
373   DH1017.IgM was nonetheless somatically mutated. The original B cell was sorted from
374   unfractionated B cells including naïve, class-switched, and non-class-switched memory B cells.

375 Naïve B cell can undergo SHM *in vitro* upon EBV transformation after prolonged culturing (≥28
376 days), often with evidence of clonal diversification, and can class-switch when stimulated with
377 CD40L and IL-21 (Heath et al., 2012), which were included in our stimulation regimen. We did not
378 identify additional nucleotide mutations or class-switched DH1017.IgG mAb from the DH1017.IgM
379 LCL throughout multiple rounds of prolonged cell expansions. Hence, while we cannot exclude
380 an origin from a naïve B cell, these observations suggest that DH1017.IgM LCL was derived from
381 an IgM+ memory B cell.

382 Structural analysis of DH1017.Fab in complex with whole ZIKV virion identified a quaternary
383 epitope footprint encompassing primarily DII that differs from that of known potently ZIKV-
384 neutralizing mAbs. Antibody responses targeting quaternary epitopes on multimeric E protein
385 epitopes or mature virions are associated with protection from ZIKV infection in mice (Maciejewski
386 et al., 2020; Metz et al., 2019). Recognition of a quaternary epitope on ZIKV is the defining feature
387 of a class of potently neutralizing mAbs (Collins et al., 2019; Hasan et al., 2017b; Long et al.,
388 2019; Rogers et al., 2017; Sapparapu et al., 2016; Stettler et al., 2016).

389 Upon viral entry into cellular endosomes, E dimers rearrange into fusogenic trimers to mediate
390 membrane fusion (Smit et al., 2011) and DH1017.IgM binding across Domain II of the E dimer
391 may cross-link ZIKV E monomers within a single dimer and restrict conformational changes to
392 prevent infection (Zhang et al., 2015). Such mechanism has also been proposed for ZIKV-117
393 and ZIKV-195 IgG mAbs (Hasan et al., 2017b; Long et al., 2019). However, our data demonstrate
394 that IgM ultrapotent neutralization is largely depended on its isotype, implying additional non-
395 mutually exclusive modes of isotype-dependent neutralization that are not available to IgG.

396 First, an IgM may efficiently cross-link multiple virions into aggregates that would not efficiently
397 internalize into cells via endosomes. Second, the large molecular size of an IgM may interfere
398 more efficiently than an IgG with virion attachment to the cell membrane and prevent cell entry.
399 Third, IgM may bind with high orders of valency to a virion by virtue of its multimeric structure,
400 thus cross-linking multiple E dimers. This could make the particle more rigid and sterically hinder
401 interactions with the cell surface to prevent either binding or fusion with the host cell. Based on
402 the position of the DH1017.IgM epitope on the i2f and q2f axes of symmetry within each
403 asymmetric unit, computational modeling of the DH1017.IgM pentamer predicts cross-linking of
404 five E dimers at the five-fold axis of symmetry resulting in a decavalent mode of antigen
405 recognition. However, concurrent cross-linking of multiple virions and competition with other ZIKV-
406 binding antibodies *in vivo* may interfere with a decavalent mode of antigen recognition on a single
407 virion. Conversely, the pentameric IgM may out compete other less avid IgG mAbs.

408 Functional results together with the potential for a multivalent mode of antigen recognition
409 suggests a functional niche that is exclusive to IgM in the context of pathogens with repetitive
410 proximal structures. The arrangement of the cognate epitope relative to the five-fold axis of
411 symmetry on the virion surface is essential for multivalent antibody interactions. Whether
412 neutralizing epitopes other than the DH1017 epitope are permissive to multivalent interactions
413 needs to be determined.

414 Intriguingly, class-switching to IgG of the DH1017.IgM clone would result in reduced function.
415 Thus, we speculate that the non-class switched IgM+ memory B cell and IgM+ plasma cell pools

416 could provide a source of neutralizing antibodies that interact with virions in an isotype-exclusive
417 manner. Future studies should address if the IgM+ memory B cell compartment is a preferential
418 source of ZIKV IgM neutralizing antibodies.

419 Neutralizing antibodies mediate protection against ZIKV as demonstrated in transfer of passive
420 immunity via immune plasma in the non-human primate model (Larocca et al., 2016; Richner et
421 al., 2017). However, IgG neutralizing antibodies at sub-neutralizing concentrations can enhance
422 flavivirus replication via ADE through FcγR mediated endocytosis of the immune complex. *In vitro*,
423 DH1017.IgG mediated ADE, whereas DH1017.IgM did not. We note that these experimental
424 results may be influenced by differences in the relative expression of FcγR and FcμR/Fcα/μR on
425 cell surface. In addition, DH1017.IgM *in vitro* neutralization potency increased in presence of
426 complement in a dose-dependent manner. Since this complement-mediated effect lowers the
427 stoichiometry requirements for neutralization, as previously reported for West Nile virus (Mehlhop
428 et al., 2009), and considering the high potency of DH1017.IgM, the risk of DH1017.IgM-mediated
429 ADE *in vivo* may be further reduced. Importantly, DH1017.IgM mediated protection against
430 subcutaneously administered lethal ZIKV challenge in mice, recapitulating protection and viral
431 control conferred by potent IgG neutralizing antibodies previously tested (Collins et al., 2019; Long
432 et al., 2019; Robbiani et al., 2017; Sapparapu et al., 2016; Swanstrom et al., 2016).

433 Since efficacy trials for ZIKV vaccines are limited by currently low levels of endemic circulation,
434 the development of prophylactic interventions that can be safely deployed to pregnant women
435 during the next ZIKV outbreak are urgently needed to mitigate the risks of congenital ZIKV
436 transmission. We propose that DH1017.IgM may be suitable as a passive intervention for
437 protection against ZIKV infection. In particular, since IgM isotype antibodies are not transferred
438 across the placenta, the potential risks of fetal toxicity and ADE in infancy after transplacental IgG
439 transfer are expected to be mitigated. Thus far, 20 IgM mAb interventions have been tested in
440 clinical trials and demonstrate that infused IgM are safe and well tolerated (Keyt et al., 2020).

441 Since the IgM half-life is considerably shorter than IgG, antibody engineering to prolong the half-
442 life would be likely required for effective prophylactic countermeasures. However, the potential
443 issue of short half-life would be less relevant for a therapeutic intervention administered at the
444 time of diagnosis, which will be aimed at rapid clearance of viremia and reduction in the time of
445 fetal exposure to circulating virus. Further, our findings support the development and investigation
446 of engineered multimeric antibody formulations as a prophylactic and therapeutic strategy.

447 In summary, we demonstrated a large contribution of plasma IgM in ZIKV neutralization in both
448 primary and DENV pre-exposed ZIKV infections in pregnancy. We isolated a novel ultrapotent
449 ZIKV-neutralizing IgM mAb that protected mice from lethal challenge and demonstrated the
450 impact of isotype on its antiviral function. We defined a conceptual framework by which the spatial
451 arrangement of quaternary epitopes on the virion can modulate neutralization in an isotype-
452 specific manner. As congenital transmission of ZIKV in pregnancy is the source of the greatest
453 burden of ZIKV disease, further studies are warranted to assess whether DH1017.IgM can protect
454 against fetal infection in pregnant animal models and mitigate fetal damage (Van Rompay et al.,
455 2020) by reducing or preventing maternal viremia. With the experience of delayed roll out of
456 vaccines to pregnant women for emerging outbreaks such as Ebola and more recently the SARS-

457 CoV-2 pandemic (Craig et al., 2021; Gomes et al., 2017), a prophylactic intervention that is rapid,
458 protective, and safe for use pregnancy will be particularly needed when ZIKV re-emerges.
459

478 **Declaration of interests:** M.B., S.R.P., T.S. and K.K.H. have filed a patent application directed
479 to antibodies that are related to this work. S.R.P. is serving as a consultant for vaccine programs
480 at Merck, Pfizer, Moderna, Dynavax and Hoopika. All other authors declare no conflict of interest.

481 **Contributions:** Conceptualization, T.S., R.D., S.R.P. and M.B.; Methodology, T.S., A.S.M.,
482 C.A.L., L.P., R.D., H.M.L., R.J.K., S.R.P. and M.B.; Investigation, T.S., K.K.H., A.S.M., R.L.J.,
483 C.A.L., M.A.G., I.M., H.S.W., J.A.E., K.L., T.V.H., R.J.E., S.V., K.E.B., S.Z., J.F.M., J.J.T., M.D.,
484 L.P. and M.B.; Resources, C.G., L.P., R.D., T.C.P., E.E.O., H.M.L., S.R.P. and M.B.; Writing –
485 Original Draft, T.S., A.S.M., S.R.P. and M.B.; Writing – Review & Editing, all authors;
486 Visualization, T.S., A.S.M., C.A.L. and M.B.; Supervision, T.C.P., E.E.O., H.M.L., R.J.K., S.R.P.
487 and M.B.; Funding Acquisition, C.A.L., C.G., R.D., H.A.L., R.J.K., S.R.P and M.B.

488

489

490

Methods

Donors and Sample Information. Participants in this study were enrolled from July 2016 to October 2017 in the city of Vitória, State of Espírito Santo, in Brazil. In this prospective cohort, we enrolled pregnant women with Zika-like symptoms of rash and/or fever and collected blood samples through pregnancy, delivery, and postpartum. Cohort design, recruitment, enrollment and sample collection are detailed in our prior study (Singh et al., 2019). Plasma and peripheral blood mononuclear cells (PBMCs) from 11 mothers who were serologically confirmed for ZIKV infection previously (Singh et al., 2019) were included in this study. The identifiers of the subjects included in this study are as follows (alternative identifiers in parenthesis): P14 (B1_0001), P15 (B1_0002), P17 (B1_0004), P19 (B1_0005), P23 (B1_0007), P24 (B1_0008), P34 (B1_0014), P50 (B1_0027), P54 (B1_0027), P56 (B1_0031) and P73 (B1_0037). The infant born to subject P14 demonstrated microcephaly at birth, and the rest had no known signs of congenital Zika syndrome. DH1017.IgM was isolated from the PBMCs of P73, who presented with a symptomatic ZIKV infection at 22 weeks of gestation and had prolonged viral replication with vRNA detected in serum/urine up to 42 DPS. She delivered an apparently healthy baby at 38.5 weeks of gestation with normal head circumference. All other mothers had detectable ZIKV vRNA in plasma at the first visit only.

Ethics Statement. The Institutional Review Boards of Hospital Cassiano Antonio Moraes (Brazilian National Research Ethics Committee (CEP/CONEP) Registration number: 52841716.0.0000.5071) and the Duke University Medical Center (Pro00100218) each approved this prospective cohort study and sampling. Pregnant women with rash or fever, who were a minimum of 18 years of age, and provided a willingness to participate through a written informed consent were approved for inclusion into this study. To protect the privacy of all subjects, publicly available identifiers are twice removed from the participant. All practices conducted as part of this study are compliant with ethical principles for medical research involving human subjects as outlined in the Declaration of Helsinki.

Animal work was approved by the University of North Carolina at Chapel Hill IACUC (protocol no. 20-132).

Cell culture and virus stocks. Vero-81 cells were grown in Dulbecco's Modified Eagle Media (Gibco 11965092) supplemented with 10% heat-inactivated fetal bovine serum (Sigma, F4135-500mL), 1x penicillin-streptomycin (Gibco 15140-122), and 1x MEM non-essential amino acids solution (Gibco 11140-050). Viruses used for the focus reduction neutralization test were DENV1 (WestPac74), DENV2 (S-16803), DENV3 (CH54389), DENV4 (TVP-360), provided by Dr. Aravinda de Silva (University of North Carolina at Chapel Hill); ZIKV H/PF/2013 and PRVABC59 strains were obtained from the Biodefense and Emerging Infections Research Resources Repository (BEI). Virion binding antibodies were detected using the following viruses from BEI: ZIKV (PRVABC59), DENV1 (Hawaii NR-82), DENV2 (New Guinea C), DENV3 (Philippines), and DENV4 (H241). ZIKV was grown in Vero-81 cells supplemented with 10% heat-inactivated fetal bovine serum (FBS) and 10mM HEPES (Sigma H0887-100ML). Dengue viruses were grown in C6/36 cells cultured in RPMI 1640 (Gibco 11875-093), L-Glutamine (Gibco 25030-081), 25 mM HEPES (Gibco, 22400-089), 1x penicillin-streptomycin (Gibco, 15140-122), and 20% FBS.

15

532 During DENV infection, RPMI was supplemented with 25mM HEPES and 2% FBS. 0.5 mL of
533 viruses were added to 80-90% confluent cells. Cells were infected with DENV2, DENV3, or
534 DENV4 for 7-9 days and DENV1 for 11 days. ZIKV stock infections were stopped when cytopathic
535 effect was observed (~3-6 day infection). Cell supernatant containing virus was then harvested,
536 centrifuged brought to a final concentration of 20% FBS, and filtered through 0.22µm filter prior
537 to storage at -80°C for use. FcγR-expressing K562 cells and THP-1 cells were maintained in RPMI
538 1640 medium containing Glutamax (Invitrogen) with 7% heat-inactivated FBS (Invitrogen) and 1X
539 penicillin-streptomycin (Invitrogen).

540 **Fluorescent labelling of ZIKV for sorting B cells.** A previously developed approach to label
541 DENV with Alexa Fluor 488 (AF488) dye was adapted to label ZIKV (Zhang et al., 2010). ZIKV
542 (Strain: PF13/251013-18) was propagated in Vero cells and purified through 30% sucrose. Virus
543 titer was determined using the BHK-21 cell plaque forming assay as previously described (Chan
544 et al., 2011). Briefly, AF488 succinimidyl ester was reconstituted in 0.2M sodium bicarbonate
545 buffer (pH 8.3) and added to 3×10^8 PFU of ZIKV at a final dye concentration of 100 µM. The
546 mixture was incubated at room temperature for 1 hour with gentle inversions every 15 minutes.
547 Labelled ZIKV was purified by size exclusion chromatography using Sephadex G-25 columns
548 (Amersham, GE Healthcare) to remove the excess dye and titrated again on BHK-21 cells.
549 Thereafter, ZIKV was UV inactivated (254nm) for 1 minute on ice. Inactivation of virus was verified
550 by serial passaging of virus on C6/36 mosquito cell line (ATCC), without detection of infection on
551 this susceptible cell line.

552 **Staining and sorting ZIKV-reactive B cells.** Thawed PBMCs were stained with Aqua Vital Dye
553 (Invitrogen), IgD-PE (clone IA6-2; BD Biosciences), CD10 PE-CF594 (clone HI10a; BD
554 Biosciences; CD3 PE-Cy5 (clone HIT3a; BD Biosciences), CD14 BV605 (clone M5E2; BD
555 Biolegend), CD16 BV570 (clone 3G8; Biolegend), CD27 PE-Cy7 (clone O323; Thermo Fisher
556 Scientific), CD38 APC-AF700 (clone LS198-4-3; Beckman Coulter), CD19 APC-Cy7 (clone
557 SJ25C1; BD Biosciences) and 1×10^6 PFU of freshly thawed UV-inactivated ZIKV labelled with
558 AF488. Additionally, 5µM of Chk2 kinase inhibitor II Inhibitor (Calbiochem/EMD Chemicals) was
559 added to prevent cell death. Unfractionated B cells were defined as CD14$^-$/CD16$^-$/CD3$^-$/CD19$^+$.
560 For memory B cells an additional IgD$^-$/CD27^{all} gate was applied. The ZIKV-reactive AF488 gate
561 was set using a fluorescence minus one condition. Cells were sorted on a Beckton Dickinson
562 FACS Aria II and analysis was performed in FlowJo.

563 **B cell cultures.** ZIKV-reactive B cells were cultured as previously described (Bonsignori et al.,
564 2011, 2016). Briefly, cells were sorted in wells pre-seeded with human CD40 ligand-expressing
565 MS40L cells (5,000 cells/well) and containing 2.5µg/ml CpG ODN2006 (tlrl-2006; InvivoGen), 5µM
566 CHK2 kinase inhibitor II) and 50 ng/ml of recombinant human (rHu) IL-21 (200-21; Peprotech) in
567 RPMI/15% fetal calf serum. EBV was added for the overnight incubation (200µl supernatant of
568 B95-8 cells per 10^4 B cells). After overnight incubation in bulk at 37°C in 5% CO_2, B cells were
569 distributed by limiting dilution at a calculated concentration of 1 cell/well into 96-well round-bottom
570 tissue culture plates in the presence of MS40L cells and complete medium described above.
571 Medium was refreshed after 7 days. Supernatants were collected after 14 days. Cell culture
572 supernatants were assessed for IgG, IgM, and IgA levels in ELISA as previously described
573 (Bonsignori et al., 2016) and Ig+ wells were further evaluated for ZIKV-reactivity with a virion

16

574 binding ELISA. From each culture well, half of the cells were harvested and preserved in RNAlater
575 (Qiagen) at day 14 and half were maintained in culture. Cell clones that immortalized were
576 expanded and cloned by using a standard limiting dilution method. Reactivity and IgV(D)J
577 sequences were checked periodically. We derived three IgG+ B-LCLs from P34 (termed 119-4-
578 D6.IgG, 119-1-D7.IgG, and 119-5-C5.IgG), three IgG+ B-LCL from P56 (124-4-C8.IgG, 124-1-
579 C2.IgG and 124-2-G3.IgG), and one IgG+ B-LCL from P54 (126-1-D11.IgG), From subject P73
580 we derived two B-LCLs: one expressing IgG from memory B cells collected 28 DPS (123-3-
581 G2.IgG), and one IgM+ B-LCL (termed DH1017) from unfractionated B cells collected at 71 DPS.

582 **Isolation of V(D)J immunoglobulin regions.** RNA from positive cultures was extracted by using
583 standard procedures (RNeasy minikit; QIAGEN), and the genes encoding Ig V_HDJ_H and
584 V_LJ_L rearrangements were amplified by RT and nested PCR without cloning by use of a previously
585 reported method (Liao et al., 2009). Ig V(D)J sequences (Genewiz) were assembled using a
586 customized bioinformatic tool developed by Kevin Wiehe (DHVI) based on the Cloanalyst
587 software package (http://www.bu.edu/computationalimmunology/research/software/).

588 **Monoclonal antibody production.** B-LCLs were expanded in CELLine bioreactor flasks
589 (Wheaton) following the manufacturer's recommendations. Monoclonal antibodies were purified
590 using protein A resin columns for IgG and CaptureSelect beads (Thermo Scientific) for
591 DH1017.IgM following manufacturer's recommendations. DH1017.IgG and DH1017.Fab heavy
592 and light chain plasmids (GenScript) were co-transfected at an equal ratio in suspension Expi
593 293i cells (Invitrogen) using ExpiFectamine 293 transfection reagents (Life Technologies)
594 according to the manufacturer's protocols. Transfected cells were gently shaken overnight for 16-
595 18 hours and incubated at 37°C with 8% CO_2. We then added the enhancer provided in the kit
596 and incubated at 37°C with 8% CO_2 for 4-6 days. Supernatant containing antibody was harvested
597 and filtered, and co-incubated with a Protein A affinity resin (Thermo Fisher Scientific) for IgG
598 antibody or LambdaFabSelect Agarose Beads (GE Healthcare Life Sciences) for Fab at 4°C on
599 a rotating shaker overnight. The bead and supernatant mixture was then loaded onto a column
600 for purification. Following a Tris/NaCl Buffer (pH 7.0) wash, mAb was eluted from beads using
601 Trizma HCl (pH 8.0; VWR) and concentrated in the Vivaspin Turbo 15 Concentrator (Thermo
602 Fisher Scientific) with a pH neutralizing buffer exchange using Citrate Buffer (pH 6.0). Purified
603 antibody concentration was determined by Nanodrop and product was evaluated by reducing and
604 nonreducing SDS-polyacrylamide gel electrophoresis and Coomassie Blue staining for
605 appropriate size.

606 **SDS PAGE and Coomassie.** DH1017.IgM was run under non-reducing conditions using a
607 NuPAGE 3-8% Tris-Acetate Gel (Invitrogen) with 1x Tris-Glycine Native Running Buffer (Novex)
608 at 130V for 2.5 hours. DH1017.IgM (5µg/lane) was prepared with Native Tris-Glycine Sample
609 Buffer (Novex) and NativeMark Protein Standard (Invitrogen) was used as the ladder. Gel was
610 subsequently stained with Coomassie and imaged using ChemiDoc (Bio-Rad).

611 **Negative stain electron microscopy.** An aliquot of DH1017.IgM was equilibrated to room
612 temperature, then diluted to 20-40 µg/ml with buffer containing 10 mM HEPES, pH 7.4, 150 mM
613 NaCl, and 0.02% ruthenium red. A 5 µl drop of diluted sample was applied to a glow-discharged
614 carbon-coated grid for 8-10 seconds, blotted, then rinsed with two drops of buffer containing 1

615   mM HEPES, pH 7.4 and 7.5 mM NaCl, and finally stained with one drop of 2% uranyl formate for
616   60 s, then blotted and air dried. Images were obtained with a Philips EM420 electron microscope
617   at 120 kV, 82,000x magnification, and captured with a 2k x 2k CCD camera at 4.02 Å/pixel. The
618   RELION program (Scheres, 2016) was used for particle picking and 2D class averaging.

619   **ZIKV and DENV virion capture ELISA.** The virion capture ELISA methods were previously
620   described (Singh et al., 2019). Briefly, high-binding 96-well plates (Greiner) were coated with 40
621   ng/well of 4G2 antibody (clone D1-4G2-4-15) in 0.1 M carbonate buffer, pH 9.6 overnight at 4°C.
622   Plates were blocked in Tris-buffered saline containing 0.05% Tween-20 and 5% normal goat
623   serum for 1 hour at 37°C, followed by an incubation with either ZIKV (PRVABC59), DENV1
624   (Hawaii), DENV2 (New Guinea C), DENV3 (Philippines), and DENV4 (H241) from BEI for 1 hour
625   at 37°C. ZIKV and DENV2 were diluted 1:5, DENV1 and DENV3 diluted 1:3, and DENV4 diluted
626   1:7. 50 µL/well samples were added and incubated for 1 hour at 37°C. Culture supernatants were
627   screened undiluted whereas plasma and purified mAb binding was measured in duplicate. Eight-
628   point serial dilutions for plasma started at 1:25 with 3-, or 5-fold dilutions and mAbs started at 100
629   ug/mL 5-fold serial dilutions. Horseradish peroxidase (HRP)-conjugated goat anti-human IgG
630   antibody (Jackson ImmunoResearch Laboratories, 109-035-008), HRP-conjugated goat anti-
631   human IgM antibody (Jackson ImmunoResearch Laboratories, 109-035-129), or HRP-conjugated
632   goat anti-human IgA antibody (Jackson ImmunoResearch Laboratories, 109-035-011) were all
633   used at a 1:5,000 dilution followed by the addition of SureBlue Reserve TMB substrate (KPL,
634   Gaithersburg, MD). Reactions were stopped by Stop Solution (KPL) after five minutes and optical
635   density (OD) was detected at 450 nm (Perkin Elmer, Victor). For IgG and IgM, an isotype matched
636   known ZIKV-specific commercial mAb was used as a positive control (IgG: C10, Absolute
637   Antibody, Cat #: AB00677-10.0; IgM: Anti NS1 IgM, myBiosource, Cat#: MBS6120634). Plasma
638   from ZIKV-infected individuals was used as positive control for IgA culture supernatants. The
639   negative control condition was sample diluent alone. Respiratory syncytial virus specific IgG
640   Palivizumab was used as a negative control for testing ZIKV-binding of purified mAbs, and diluent
641   served as negative control for IgM purified mAb assays. For purified mAbs that were serially
642   diluted, the magnitude of virion binding was evaluated as an ED_{50}, which was calculated with a
643   sigmoidal dose-response (variable slope) curve in Prism 7 (GraphPad) using a least squares fit.
644   The ED_{50} value for serially diluted mAbs was considered valid if the OD_{450} at 100ug/mL was 5-
645   fold higher than the no sample condition. For plasma, the ED_{50} value was considered valid if the
646   OD_{450} at 1:25 dilution 2 standard deviations above the mean OD_{450} for DENV 1-4, and 3 standard
647   deviations above the mean OD_{450} observed for 11 plasma samples from healthy U.S. subjects
648   (2SD OD_{450} cut-offs: DENV-1 = 0.406, DENV-2 = 0.648, DENV3 = 0.906, and DENV-4 = 0.885;
649   3SD OD_{450} cut-off: ZIKV = 0.596). For culture supernatants, the cut-off for positivity was the
650   highest of mean plate blanks OD_{450} + 2 standard deviations and OD_{450} not less than 0.4.

651   **Recombinant E protein ELISA.** DH1017 mAbs was immobilized to a high-binding 96-well plate
652   (Greiner) at 0.5ug/mL in 1x TBS, then blocked with 3% milk in TBS tween, each for 1 hour at
653   37°C. Serial dilutions of his-tagged recombinant E protein dimer (Premkumar et al., 2017) starting
654   at 20ug/mL with 2-fold dilutions to 12-spots were added to the plate for an hour at 37°C. This was
655   followed by 0.5ug/mL anti-his HRP (Sigma), and binding was detected after incubation with
656   substrate at an absorbance of 450nm. EC_{50} was obtained by a sigmoidal dose-response (variable

657 slope) curve in Prism 7 (GraphPad) using least squares fit. The negative control was no antigen
658 and positive control were previously reported mAbs, including 1M7, ZV-2, ZV-64 and ZKA190.
659 1M7 mAb (Smith et al., 2013) was produced from a hybridoma. ZKA190 was generated
660 recombinantly using the sequence for PDB entry 5Y0A (Wang et al., 2017). The mouse mAbs
661 ZV-2 and ZV-64 (Zhao et al., 2016) were produced from hybridomas at the UNC protein
662 expression core facility. ZIKA-752, ZIKA-893, and rZIKV-195 were produced and provided by
663 James Crowe.

664 **Focus reduction neutralization test.** We used previously described methods for $FRNT_{50}$ in a
665 96-well plate (Singh et al., 2019). Briefly, serial dilutions of heat-inactivated plasma or purified
666 mAbs were added to 30-60 focus forming units of either DENV serotypes 1-4 or ZIKV
667 (H/PF/2013). Plasma was used at a starting dilution of 1:25 with subsequent 5-fold or 7-fold
668 dilutions. MAbs were tested at 5ug/mL or 10ug/mL with 5-fold dilution series. However,
669 DH1017.Fab, was tested at 1mg/mL with a 5-fold dilution series. Negative control was media
670 alone, and positive controls were known ZIKV-neutralizing mAbs and plasma from ZIKV-infected
671 subjects. Virus and plasma or mAb samples were co-incubated for 1 hour at 37°C, then
672 transferred to a 96-well plate (Greiner Bio One) with confluent Vero-81 cells and incubated for 1
673 hour at 37°C. Plates were overlayed with 1% methylcellulose and incubated at 37°C for 40-42
674 hours (ZIKV and DENV4), 51-53 hours (DENV1), or 48 hours (DENV2 and DENV3). Cells were
675 fixed with 2% paraformaldehyde for 30 minutes and stained with 0.5 µg/mL of 4G2 or E60 mouse
676 monoclonal antibody. Foci were detected with an anti-mouse IgG conjugated to horseradish
677 peroxidase at a 1:5000 dilution (Sigma), followed by True Blue substrate (KPL). Foci were
678 counted using the CTL ImmunoSpot plate reader (Cellular Technology Limited). $FRNT_{50}$ values
679 were calculated with the sigmoidal dose-response (variable slope) curve in Prism 8.3.0
680 (GraphPad), constraining values between 0 and 100% relative infection. Percent relative infection
681 curves were considered to pass quality control criteria for $FRNT_{50}$ determination if $R^2 > 0.65$,
682 absolute value of hill slope >0.5, and curve crossed 50% relative infection within the range of the
683 plasma dilutions in the assay. Samples were repeated up to 3 times to quantify a valid $FRNT_{50}$ in
684 accordance with the quality control criteria.

685 **Reporter Virus Particle (RVP) production.** ZIKV RVPs incorporating the structural proteins
686 (Capsid [C], premembrane [prM], and E) of ZIKV strain H/PF/2013 were produced by genetic
687 complementation of a green fluorescent protein (GFP)-expressing WNV lineage II sub-genomic
688 replicon with the virus structural gene plasmids as previously described (Dowd et al., 2016).
689 Briefly, the WNV replicon and C-prM-E plasmids were co-transfected into HEK-293T cells using
690 Lipofectamine 3000™ transfection reagent (Invitrogen). Transfected cells were incubated at 30°C
691 and RVP-containing supernatants were harvested 3-6 days post-transfection and pooled. RVP-
692 containing supernatants were passed through a 0.2 µm filter (Millipore) and stored at -80°C until
693 use.

694 **RVP-based Antibody-Dependent Enhancement (ADE) assay.** RVP-based ADE assays were
695 performed by incubating GFP-encoding RVPs with serial dilutions of mAbs for 1 h at 37°C. FcγR+
696 K562 or THP-1 cells were infected with RVP immune complexes and incubated at 37°C for 36-
697 48 h. Cells were fixed with paraformaldehyde, and GFP expression was detected by flow
698 cytometry. Antibody enhanced infection was scored as detectable if the number of GFP positive

699   cells was ≥3-fold above background (defined as the average percent GFP positive cells in the
700   absence of antibody).

701   **Plaque assay-based ADE assay.** DH1017.IgM and DH1017.IgG were serially diluted 2-fold over
702   6.25 – 0.003 µg/mL and 10uL of diluted mAb were co-incubated in duplicate with 2 x 10^5 PFU of
703   ZIKV (Strain: PD13/251013-18) in a round bottom 96 well-plate for 1 hour at 37ºC to form immune
704   complexes. Thereafter, 2 x 10^4 cells of THP1.2S or primary monocytes were added to the ZIKV
705   and mAb immune complexes for a 72-hour multiday infection at 37ºC. THP1.2S cells are a
706   subclone of the THP1 monocyte cell line (ATCC) that are shown to be more susceptible to
707   flavivirus infection (Chan et al., 2014). Collection and processing of primary monocytes has been
708   previously described and was conducted approval of the NUS Institutional Review Board under
709   reference code B-15-227 (Chan et al., 2019). After the multiday infection on monocytes,
710   supernatant was collected, and infectious virus was tittered via plaque forming assays on BHK-1
711   cells (ATCC) in 24 well plates in quadruplicate, as previously described (Chan et al., 2011). For
712   the positive control we used humanized IgG1 4G2 mAb, and for the negative control we used 3H5
713   (DENV-specific mAb) as well as the virus only condition, without any mAb present.

714   **Antibody-dependent complement antiviral activity.** Focus reduction neutralization test
715   (FRNT) in the presence of increasing concentrations [volume/volume] of complement from normal
716   human serum (Sigma), including 0, 5, 10, 15, 20 and 25% final concentration were tested. Percent
717   relative infection was calculated as a ratio of the foci in the plasma, ZIKV (PRVABC59), and
718   complement condition, to the foci in the virus and complement condition, multiplied by 100. This
719   approach allows for determination of the antibody-dependent complement activity and adjusts for
720   antibody-independent complement activity. Samples were run in triplicate and experiment was
721   independently repeated for each concentration of complement. Positive control was DH1017.IgM
722   and DH1017.IgG run in the absence of complement, and negative control was the virus and
723   complement only conditions. The rest of the analysis and approach are identical to the FRNT
724   approach.

725   **Determining the contribution of plasma IgM to ZIKV neutralization.** Each original plasma
726   sample was split into 2 aliquots, with one portion depleted of IgM isotype antibodies and another
727   portion mock depleted. First, each sample was heat inactivated for 30 minutes at 56ºC, diluted
728   1:1 with sterile PBS, and centrifuged at 10,000 x G for 10 minutes to remove debris. Depletion
729   beads were packed into sterile 0.5mL centrifugal filter devices with a 0.22µm pore PVDF
730   membrane (Millipore) and equilibrated with 3x sterile PBS washes (pH 7.2). 200mg of POROS™
731   CaptureSelect™ IgM affinity beads (ThermoFisher Scientific) were used for IgM depletion, and
732   66mg of corresponding beads of the same size (200-400 mesh) and material (polystyrene
733   divinylbenzene 1% cross linked beads; Alfa Aesar) were used for mock depletion. Samples were
734   co-incubated with beads for 10 minutes at room temperature with gentle inversions, and then the
735   depleted fraction was centrifuged at 10,000 x g for 10 minutes.

736   Depletion of IgM was confirmed by total IgM ELISA, and non-specific losses to ZIKV-binding IgG
737   were quantified through virion binding ELISA; both assays are described in other sections of this
738   Method supplement. Limit of detection (LOD) of 0.12 µg/mL was based on the linear range of a
739   sigmoidal standard curve of human IgM (Jackson ImmunoResearch Laboratories). Magnitude of

20

740 ZIKV-binding IgG was assessed by virion-binding ELISA and neutralization potency was
741 assessed using the Focus Reduction Neutralization Test. Due to slight differences in ZIKV-
742 binding IgG across IgM and mock depleted fractions, each fraction was adjusted to the magnitude
743 of ZIKV-binding IgG in the same sample such that differences in neutralization activity could be
744 attributed to differences in IgM isotype antibodies. Thus, the percent neutralization attributable to
745 IgM that is reported in this study was calculated as follows:

746
$$ZIKV\ IgG\ normalized\ ZIKV\ neutralization\ (\boldsymbol{nFRNT_{50}})$$

747
$$= \frac{ZIKV\ neutralizing\ titer\ (FRNT_{50})}{ZIKV\ specific\ IgG\ (ED_{50})}$$

748

749
$$Percent\ ZIKV\ neutralization\ attributable\ to\ IgM\ (\%)$$

750
$$= 100 \times \frac{Mock\ depleted\ nFRNT_{50}\ -\ IgM\ depleted\ nFRNT_{50}}{Mock\ depleted\ nFRNT_{50}}$$

751 **Detection of antibody isotype from sera.** Human IgM antibodies were detected in sera from
752 passively transferred mice using high-binding 384-well plates (VWR) coated with 0.5 μg/well of
753 goat anti-human Ig polyvalent antibody (ThermoFisher, #H17000) in 0.1 M carbonate buffer, pH
754 9.6 overnight at 4°C. Plates were blocked the next day (2 hours at RT) with 10X PBS containing
755 4% whey, 15% normal goat serum, and 0.5% tween. Mouse serum samples were diluted 1:30,
756 serially diluted three-fold, then added to the plate (10μL/well), and incubated for 1 hour at 37°C.
757 Horseradish peroxidase (HRP)- conjugated goat anti-human IgM antibody (Jackson
758 ImmunoResearch Laboratories, 109-035-129) was used at a 1:10,000 dilution (10μL/well)
759 followed by the addition of SureBlue Reserve TMB substrate (KPL). Reactions were stopped by
760 Stop Solution (KPL, Gaithersburg, MD) after five minutes and optical density (OD) was detected
761 at 450 nm (Perkin Elmer, Victor). DH1017.IgM was used as a positive control and standard. Blank
762 wells were used as a negative control. Antibody concentrations were interpolated from the
763 standard curve, which was fit using to a 5-parameter fit sigmoidal curve (SoftMax Pro 6.3;
764 Molecular Devices). Concentrations were interpolated from OD_{450} values within the linear range
765 of the sigmoidal curve at dilution 90, or alternatively 30, for samples at 2-6 DPI, and at dilution 10
766 for samples at 8+ DPI. A passing quality control criterion of replicate OD_{450} values less than or
767 equal to 25% variance was applied. Limit of detection for this assay was 0.08 μg/mL across
768 assays, based on the linear range of the standard curve.

769 To measure concentration of IgM from human plasma, the same assay was applied with the
770 following modifications. All original and IgM/mock depleted samples were diluted 1:30 relative to
771 original plasma with 3-fold serial dilutions. Human IgM (Jackson ImmunoResearch Laboratories,
772 009-000-012) was used as positive control and standard. IgM concentration in sample was
773 inferred based upon the 1:2430, or alternatively the 1:270 and 1:810 serum dilutions, which were
774 all in the linear range of the standard curve.

775 **Biolayer interferometry.** BLI assays were performed on the ForteBio Octet Red96 instrument at
776 25ºC with a shake speed of 1,000 RPM. Goat Anti-Human Ig polyvalent (20 μg/mL; Thermo

21

777 Fisher) was amine coupled to AR2G sensor tips as follows: sensor tips were activated with s-
778 NHS/EDC (300s), incubated in Anti-Human Ig (600s), and quenched with ethanolamine (300s).
779 DH1017.IgM, DH1017.IgG, and a negative control IgG (palivizumab) were diluted to 50μg/mL in
780 PBS and captured on the biosensors (300s), followed by a PBS wash (60s). A baseline signal
781 was recorded for 2 min in PBS (pH 7.4). Biosensors were then immersed into a two-fold dilution
782 series of ZIKV E protein dimer in PBS (50-0.78μg/mL) to measure association (400s), followed
783 by immersion into PBS to measure dissociation (600s). All binding profiles were corrected by
784 double reference subtraction using the signal obtained in a PBS control (without E proteins) and
785 the signal obtained from the Palivizumab control sensor. All affinities were calculated using the
786 fast kinetic components of the heterogeneous ligand model fit. Kinetics and affinity data are the
787 result of a single measurement.

788 **Size exclusion chromatography.** ZIKV E dimer was screened for size on Superdex 200 Inc
789 10/300 GL column: 100uL of E dimer was loaded onto the column at 0.13mg/mL and was run at
790 a flow rate of 0.5 mL/min in PBS.

791 **Virus propagation and purification for cryo electron microscopy.** ZIKV strain H/PF/2013
792 was propagated in Vero-Furin cells (Mukherjee et al., 2016). Approximately 10^9 Vero-Furin cells,
793 grown in 10% FBS (Sigma, F0926), Dulbecco's modified Eagle medium (DMEM) media
794 (Thermofisher, 41300039) and 50 ug/mL blasticidin (Invivogen, anti-bl-1) at 37°C 5% CO_2, were
795 infected with a MOI of 0.1. Virus particles in 2% FBS/DMEM/1mM Pen/Strep (Thermofisher,
796 15140122) were incubated with cells for 2 hours at room temperature. After 2 hours, infected cells
797 were incubated at 37°C, 5% CO_2 for 36 hours. At 36 hours post infection (hpi), infectious media
798 was collected and replaced with fresh media every 12 hours up to 84 hpi. Virus particles were
799 purified from media collected at 60 and 72 hpi.

800 Briefly, cell debris were pelleted by centrifugation at 2,744 x g for 30 minutes. Infectious media
801 was filtered with through a Steritop-GP 0.2 μm filter (Millipore, SCGPT05RE) and virus particles
802 were precipitated overnight at 4°C with PEG 4000, 8% final concentration. PEG precipitated
803 particles were concentrated at 8,891 x *g* for 50 minutes. Particles were concentrated through a
804 24% sucrose cushion by ultra-centrifugation at 126,144 x *g* for 2 hours at 4°C. Virus particles
805 were isolated with a discontinuous potassium-tartrate/glycerol/NTE buffer (120mM NaCl, 20mM
806 Tris pH 8.0, 1mM EDTA) gradient in 5% increments between 35% and 10% potassium-tartrate
807 and ultra-centrifugation at 126,144 x *g* for 2 hours at 4C. The particles were extracted from the
808 20% fraction of the discontinuous gradient and buffer exchanged and concentrated in NTE buffer
809 with a 100 kDa MWCO centrifugal filter.

810 **Single particle cryoelectron microscopy.** Prior to freezing, purified virus and DH1017.Fab
811 fragments were incubated on ice for 2 hours at a molar ratio of 0.2 mM Fab to 1 mM E protein.
812 Samples were then plunge frozen in liquid ethane using a Cryoplunge 3 System (GATAN). Briefly,
813 liquid nitrogen was used to liquefy ethane at -190°C. A 2.5μL volume of sample was spotted on
814 lacey carbon grids (Ultrathin C on Lacey Carbon Support film, 400 mesh, Cu. Ted Pella, Inc.
815 Product number 01824) and blotted with Whatman grade 1, 200mm circle filter paper (GE
816 Healthcare Life Sciences, catalog number 1001-020) for 2.5 seconds. Blotting air pressure setting
817 used was 100 psi.

818   Data were collected on a Titan Krios (Thermofisher) microscope equipped with a Gatan K3
819   detector using and Leginon software package (Suloway et al., 2005). A total of 1,929 cryo EM
820   micrographs were collected with a nominal magnification of 64000x, 0.66 Å/pixel size, and an
821   electron dose equivalent, of 35 e-/Å2. Motion correction and CTF calculations estimations were
822   performed using MotionCorr2 (Zheng et al., 2017) and CTFFIND4 (Rohou and Grigorieff, 2015)
823   respectively.

824   Automated particle selection picking (Sigworth, 2004) performed with cisTEM (Grant et al., 2018)
825   selected 34,474 particles. A maximum-likelihood algorithm based 2D classification (Scheres et
826   al., 2005; Sigworth, 1998) was performed with using cisTEM. From a subset of 2D classes, 4104
827   particles were selected for further processing.

828   Single particle reconstruction was performed according to the 'gold standard' method using jspr
829   (Guo and Jiang, 2014). Briefly, the particles were divided equally into two randomly selected
830   independent particle sets. Twenty ab-initio models were generated from a random set of 700
831   particles selected from the set of 4,104 particles. Two ab-initio models were selected, and one
832   ab-initio model was assigned to one independent particle set and the other ab-initio model was
833   assigned to the other independent data set. Each dataset was refined iteratively assuming
834   icosahedral symmetry. Refinement resulted in two independent models that converged on the
835   same structure. Following corrections for astigmatism, elliptical distortion, defocus, and the
836   masking of the disordered nucleocapsid core, the final models of each independent data set were
837   combined into a single final model. The resolution of the map was calculated at 0.143 from the
838   FSC curve (Rosenthal and Henderson, 2003).

839   **Model fitting, refinement, and structure analysis.** Models used in fitting viral structural proteins
840   in the cryo EM density map are the E glycoprotein ectodomain of the ZIKV asymmetric unit (PDB
841   6CO18) (Sevvana et al., 2018) and a homology model of DH1017.Fab fragment. The Fab
842   fragment model is composed of individual domains variable heavy, variable light, C, and lambda
843   domains. The homology models of each Fab fragment domain were generated with I-TASSER
844   (Roy et al., 2010; Yang et al., 2014; Zhang, 2008) and aligned with PYMOL (version 2.0,
845   Schrodinger LLC) to an IgM cryoglobulin Fab crystal structure (PDB 2AGJ) (Ramsland et al.,
846   2006) to form the complete DH1017.Fab homology model. The C_α backbones of all structures
847   were fit in the cryo-EM map using Chimera (Pettersen et al., 2004) fit-to-map function. The
848   position of the Fab domains was further refined with Coot (Emsley, P 2010). Residues of the E
849   ectodomain C_α backbone within 6 Å of the Fab fragment C_α backbone were identified with
850   PYMOL. These residues are defined as the Fab footprint and mapped to the surface of the virus
851   particle with RIVEM (Xiao and Rossmann, 2007). The binding of a human IgM pentamer to the
852   virus surface at the five-fold icosahedral axis was modeled. The solution structure of an IgM
853   pentamer (PDB 2CRJ) (Perkins et al., 1991) and the homology model of DH1017.Fab from this
854   paper were used to build the model. The Fc domains Cμ4, Cμ3, and Cμ2 of PDB 2CRJ were
855   modeled to similar positions of Cμ4 (PDB 4JVW), Cμ3 (PDB 4BA8), and Cμ2 (4JVU) domains fit
856   to the 25A tomogram of an IgM pentamer bound to the surface of an artificial liposome (Müller et
857   al., 2013; Sharp et al., 2019). One Fab domain from each monomer of the pentamer structure
858   PDB 2CRJ were fit to the density map after being aligned manually to the fitted DH1017.Fab
859   structure.

Assessing protection in ZIKV mouse model. Animal husbandry and experiments were performed under the approval of the University of North Carolina at Chapel Hill Institutional Animal Care and Use Committee. Five-week-old male $Ifnar1^{-/-}$ mice were inoculated with a lethal dose of ZIKV strain H/PF/2013 (1×10^3 FFU) subcutaneously in the footpad on day 0 (Lazear et al., 2016). On days -1 and +1, 100μg of antibody was delivered intravenously via the retro-orbital route. Serum was collected every two days for 11 days to monitor viremia by qRT-PCR and survival was monitored for 15 days. Animals that lost ≥30% of their starting weight or that exhibited severe disease signs were euthanized.

Measuring viral burden in mice. RNA from the serum of ZIKV-infected mice was extracted with the Qiagen viral RNA minikit. ZIKV RNA was quantified by TaqMan one-step qRT-PCR using a CFX96 Touch real-time PCR detection system (Bio-Rad). Genome copies per mL of serum on a log_{10} scale was determined by comparison with a standard curve generated by using serial 10-fold dilutions of a ZIKV plasmid and previously reported primers: forward primer CCGCTGCCCAACACAAG, reverse primer CCACTAACGTTCTTTTGCAGACAT, and probe 5′-FAM (6-carboxyfluorescein)-AGCCTACCT-ZEN-TGACAAGCAATCAGACACTCAA-3′IABkFQ (Integrated DNA Technologies) (Carbaugh et al., 2019)**.**

Reactivity to autoantigens. ELISA was performed in 384-well plates (Corning) as previously described (Bonsignori et al., 2011). Briefly, plates were coated overnight at 4°C with 15μl purified proteins at optimized concentrations in 0.1M Sodium Bicarbonate: DNA (Worthington, LS002105) at 5μg/mL, Centromere B (Prospec, PRO-390) at 0.15μg/mL, Histone (Sigma, H9250) at 0.2μg/mL, Jo-1 (Immunovision, JO1-3000) at 0.05 units/well, RnP/Sm (Immunovision, SRC-3000) at 0.2 units/well, Scl-70 (Immunovision, SCL-3000) at 0.4 units/well, Sm (Immunovision, SMA-3000) at 0.1 units/well, SSA (Immunovision, SSA-3000) at 0.2 units/well, and SSB (Immunovision, SSB-3000) at 0.1 units/well. Subsequently, plates were blocked (50μL/well) with assay diluent (PBS containing 4% [w/v] whey protein, 15% normal goat serum, 0.5% Tween 20) for 2 hours at room temperature. For DNA, plates were pre-coated with Poly-L-Lysine (Sigma, P6282) at 2μg/mL in PBS overnight at 4°C, and the assay diluent was PBS containing 2% [w/v] bovine serum albumin and 0.05% Tween-20. Monoclonal antibodies were tested using 3-fold serial dilutions starting at 10μg/ml. 10μl of primary antibodies were added to each well and incubated for 1 hour at room temperature. The following positive control antibodies from Immunovision were all tested at a 1:25 starting dilution with 3-fold serial dilutions: Anti-Centromere B (HCT-0100), Anti-single stranded DNA (HSS-0100), Anti-Histone (HIS-0100), Anti-Jo 1 (HJO-0100), Anti-SRC (HRN-0100), Anti-Scl 70 (HSC-0100), Anti-Sm (HSM-0100), Anti-SSA (HSA-0100), and Anti-SSB (HSB-0100). The negative control was assay diluent alone. Plates were developed using 15μl/well of combination of horseradish peroxidase–conjugated antibodies in assay diluent comprising) goat anti-human IgG (Jackson ImmunoResearch Laboratories,109-035-098) at 1:10,000 dilution; 2) goat anti-human IgM (Jackson ImmunoResearch Laboratories,109-035-129) at 1:10,000 dilution; 3) goat anti-human H+L (Promega, W403B) at 1:3,000 dilution. After a 1 hour incubation, plates were developed with 20μl/well of SureBlue Reserve TMB substrate (KPL) and stopped by 20μl/well Stop Solution (KPL) after five minutes. Optical density (OD) was detected at 450 nm (Perkin Elmer, Victor).

901   **HEp-2 Cell Staining.** Indirect immunofluorescence (Zeuss Scientific) binding of DH1017 mAbs
902   to HEp-2 cells was performed as previously described (Bonsignori et al., 2014). IgG1 mAbs 2F5
903   and 17B were used as positive and negative controls, respectively. All mAbs were tested at
904   25ug/ml and 50ug/mL. Images were acquired for 8 seconds with a 40x objective.

References

905

906 Abbink, P., Larocca, R.A., De La Barrera, R.A., Bricault, C.A., Moseley, E.T., Boyd, M., Kirilova,
907 M., Li, Z., Ng'ang'a, D., Nanayakkara, O., et al. (2016). Protective efficacy of multiple vaccine
908 platforms against Zika virus challenge in rhesus monkeys. Science (80-.). *353*, 1129–1132.

909 Bonsignori, M., Hwang, K.-K., Chen, X., Tsao, C.-Y., Morris, L., Gray, E., Marshall, D.J., Crump,
910 J.A., Kapiga, S.H., Sam, N.E., et al. (2011). Analysis of a Clonal Lineage of HIV-1 Envelope
911 V2/V3 Conformational Epitope-Specific Broadly Neutralizing Antibodies and Their Inferred
912 Unmutated Common Ancestors. J. Virol. *85*, 9998–10009.

913 Bonsignori, M., Wiehe, K., Grimm, S.K., Lynch, R., Yang, G., Kozink, D.M., Perrin, F., Cooper,
914 A.J., Hwang, K.K., Chen, X., et al. (2014). An autoreactive antibody from an SLE/HIV-1
915 individual broadly neutralizes HIV-1. J. Clin. Invest. *124*, 1835–1843.

916 Bonsignori, M., Zhou, T., Sheng, Z., Chen, L., Gao, F., Joyce, M.G., Ozorowski, G., Chuang,
917 G.Y., Schramm, C.A., Wiehe, K., et al. (2016). Maturation Pathway from Germline to Broad HIV-
918 1 Neutralizer of a CD4-Mimic Antibody. Cell *165*, 449–463.

919 Bonsignori, M., Scott, E., Wiehe, K., Easterhoff, D., Alam, S.M., Hwang, K.K., Cooper, M., Xia,
920 S.M., Zhang, R., Montefiori, D.C., et al. (2018). Inference of the HIV-1 VRC01 Antibody Lineage
921 Unmutated Common Ancestor Reveals Alternative Pathways to Overcome a Key Glycan
922 Barrier. Immunity *49*, 1162-1174.e8.

923 Calvert, A.E., Horiuchi, K., Boroughs, K.L., Ong, Y.T., Anderson, K.M., Biggerstaff, B.J., Stone,
924 M., Simmons, G., Busch, M.P., and Huang, C.Y.-H. (2021). The Specificity of the Persistent IgM
925 Neutralizing Antibody Response in Zika Viral Infections Among Individuals with Prior Dengue
926 Virus Exposure. J. Clin. Microbiol.

927 Campos, M.C., Dombrowski, J.G., Phelan, J., Marinho, C.R.F., Hibberd, M., Clark, T.G., and
928 Campino, S. (2018). Zika might not be acting alone: Using an ecological study approach to
929 investigate potential co-acting risk factors for an unusual pattern of microcephaly in Brazil. PLoS
930 One *13*, e0201452.

931 Carbaugh, D.L., Baric, R.S., and Lazear, H.M. (2019). Envelope Protein Glycosylation Mediates
932 Zika Virus Pathogenesis. J. Virol. *93*.

933 Chan, C.Y.Y., Low, J.Z.H., Gan, E.S., Ong, E.Z., Zhang, S.L.-X., Tan, H.C., Chai, X., Ghosh, S.,
934 Ooi, E.E., and Chan, K.R. (2019). Antibody-Dependent Dengue Virus Entry Modulates Cell
935 Intrinsic Responses for Enhanced Infection. MSphere *4*, 528–547.

936 Chan, K.R., Zhang, S.L.-X., Tan, H.C., Chan, Y.K., Chow, A., Lim, A.P.C., Vasudevan, S.G.,
937 Hanson, B.J., and Ooi, E.E. (2011). Ligation of Fc gamma receptor IIB inhibits antibody-
938 dependent enhancement of dengue virus infection. Proc. Natl. Acad. Sci. *108*, 12479–12484.

939 Chan, K.R., Ong, E.Z., Tan, H.C., Zhang, S.L.-X., Zhang, Q., Tang, K.F., Kaliaperumal, N., Lim,
940 A.P.C., Hibberd, M.L., Chan, S.H., et al. (2014). Leukocyte immunoglobulin-like receptor B1 is
941 critical for antibody-dependent dengue. Proc. Natl. Acad. Sci. U. S. A. *111*, 2722–2727.

942 Chan, K.R., Ong, E.Z., Mok, D.Z.L., and Ooi, E.E. (2015). Fc receptors and their influence on
943 efficacy of therapeutic antibodies for treatment of viral diseases. Expert Rev. Anti. Infect. Ther.
944 *13*, 1351–1360.

945 Christiansen, J.S., Andersen, A.R., Osther, K., Peitersen, B., Bach-Mortensen, N., and Lebech,
946 P.E. (1976). THE RELATIONSHIP BETWEEN PREGNANCY, HCS AND B LYMPHOCYTES.

947 Acta Pathol. Microbiol. Scand. Sect. C Immunol. *84 C*, 313–318.

948 Chua, C.-L., Sam, I.-C., Chiam, C.-W., and Chan, Y.-F. (2017). The neutralizing role of IgM
949 during early Chikungunya virus infection. PLoS One *12*, e0171989.

950 Collins, M.H., Tu, H.A., Gimblet-Ochieng, C., Liou, G.J.A., Jadi, R.S., Metz, S.W., Thomas, A.,
951 McElvany, B.D., Davidson, E., Doranz, B.J., et al. (2019). Human antibody response to Zika
952 targets type-specific quaternary structure epitopes. JCI Insight *4*.

953 Craig, A.M., Hughes, B.L., and Swamy, G.K. (2021). Coronavirus disease 2019 vaccines in
954 pregnancy. Am. J. Obstet. Gynecol. MFM *3*, 100295.

955 Diamond, M.S., Sitati, E.M., Friend, L.D., Higgs, S., Shrestha, B., and Engle, M. (2003). A
956 Critical Role for Induced IgM in the Protection against West Nile Virus Infection. J. Exp. Med.
957 *198*, 1853–1862.

958 Gasser, R., Cloutier, M., Prévost, J., Fink, C., Ducas, É., Dussault, N., Landry, P., Tremblay, T.,
959 Laforce-Lavoie, A., Lewin, A., et al. (2020). Major role of IgM in the neutralizing activity of
960 convalescent plasma against SARS-CoV-2. BioRxiv 2020.10.09.333278.

961 Gibney, K.B., Edupuganti, S., Panella, A.J., Kosoy, O.I., Delorey, M.J., Lanciotti, R.S., Mulligan,
962 M.J., Fischer, M., and Staples, J.E. (2012). Detection of anti-yellow fever virus immunoglobulin
963 M antibodies at 3-4 years following yellow fever vaccination. Am. J. Trop. Med. Hyg. *87*, 1112–
964 1115.

965 Gilchuk, P., Bombardi, R.G., Erasmus, J.H., Tan, Q., Nargi, R., Soto, C., Abbink, P., Suscovich,
966 T.J., Durnell, L.A., Khandhar, A., et al. (2020). Integrated pipeline for the accelerated discovery
967 of antiviral antibody therapeutics. Nat. Biomed. Eng. *4*, 1030–1043.

968 Gomes, M.F., De La Fuente-Núñez, V., Saxena, A., and Kuesel, A.C. (2017). Protected to
969 death: Systematic exclusion of pregnant women from Ebola virus disease trials. Reprod. Health
970 *14*.

971 Grant, T., Rohou, A., and Grigorieff, N. (2018). CisTEM, user-friendly software for single-particle
972 image processing. Elife *7*.

973 Griffin, I., Martin, S.W., Fischer, M., Chambers, T. V., Kosoy, O.L., Goldberg, C., Falise, A.,
974 Villamil, V., Ponomareva, O., Gillis, L.D., et al. (2019). Zika virus IGM 25 months after symptom
975 onset, Miami-Dade County, Florida, USA. Emerg. Infect. Dis. *25*, 2264–2265.

976 Guo, F., and Jiang, W. (2014). Single particle cryo-electron microscopy and 3-D reconstruction
977 of viruses. Methods Mol. Biol. *1117*, 401–443.

978 Halstead, S.B. (1988). Pathogenesis of dengue: Challenges to molecular biology. Science (80-.
979). *239*, 476–481.

980 Halstead, S.B., and O'Rourke, E.J. (1977). Antibody-enhanced dengue virus infection in primate
981 leukocytes [21]. Nature *265*, 739–741.

982 Hasan, S.S., Miller, A., Sapparapu, G., Fernandez, E., Klose, T., Long, F., Fokine, A., Porta,
983 J.C., Jiang, W., Diamond, M.S., et al. (2017a). A human antibody against Zika virus crosslinks
984 the E protein to prevent infection. Nat. Commun. *8*, 14722.

985 Hasan, S.S., Miller, A., Sapparapu, G., Fernandez, E., Klose, T., Long, F., Fokine, A., Porta,
986 J.C., Jiang, W., Diamond, M.S., et al. (2017b). A human antibody against Zika virus crosslinks
987 the E protein to prevent infection. Nat. Commun. *8*, 1–6.

27

988 Heath, E., Begue-Pastor, N., Chaganti, S., Croom-Carter, D., Shannon-Lowe, C., Kube, D.,
989 Feederle, R., Delecluse, H.-J., Rickinson, A.B., and Bell, A.I. (2012). Epstein-Barr Virus
990 Infection of Naïve B Cells In Vitro Frequently Selects Clones with Mutated Immunoglobulin
991 Genotypes: Implications for Virus Biology. PLOS Pathog. *8*, e1002697.

992 Hensel, F., Timmermann, W., Von Rahden, B.H.A., Rosenwald, A., Brändlein, S., and Illert, B.
993 (2014). Ten-year follow-up of a prospective trial for the targeted therapy of gastric cancer with
994 the human monoclonal antibody PAT-SC1. Oncol. Rep. *31*, 1059–1066.

995 Hombach, J., Solomon, T., Kurane, I., Jacobson, J., and Wood, D. (2005). Report on a WHO
996 consultation on immunological endpoints for evaluation of new Japanese encephalitis vaccines,
997 WHO, Geneva, 2-3 September, 2004. Vaccine *23*, 5205–5211.

998 Katzelnick, L.C., Harris, E., Baric, R., Coller, B.A., Coloma, J., Crowe, J.E., Cummings, D.A.T.,
999 Dean, H., De Silva, A., Diamond, M.S., et al. (2017). Immune correlates of protection for
1000 dengue: State of the art and research Agenda. In Vaccine, (Elsevier Ltd), pp. 4659–4669.

1001 Keyt, B.A., Baliga, R., Sinclair, A.M., Carroll, S.F., and Peterson, M.S. (2020). Structure,
1002 Function, and Therapeutic Use of IgM Antibodies. Antibodies *9*, 53.

1003 King, H.W., Orban, N., Riches, J.C., Clear, A.J., Warnes, G., Teichmann, S.A., and James, L.K.
1004 (2021). Single-cell analysis of human B cell maturation predicts how antibody class switching
1005 shapes selection dynamics. Sci. Immunol. *6*.

1006 Kreil, T.R., Burger, I., Bachmann, M., Fraiss, S., and Eibl, M.M. (1997). Antibodies protect mice
1007 against challenge with tick-borne encephalitis virus (TBEV)-infected macrophages. Clin. Exp.
1008 Immunol. *110*, 358–361.

1009 Kwek, S. Sen, Watanabe, S., Chan, K.R., Ong, E.Z., Tan, H.C., Ng, W.C., Nguyen, M.T.X.,
1010 Gan, E.S., Zhang, S.L., Chan, K.W.K., et al. (2018). A systematic approach to the development
1011 of a safe live attenuated Zika vaccine. Nat. Commun. *9*, 1031.

1012 Larocca, R.A., Abbink, P., Peron, J.P.S., Zanotto, P.M.D.A., Iampietro, M.J., Badamchi-Zadeh,
1013 A., Boyd, M., Ng'ang'a, D., Kirilova, M., Nityanandam, R., et al. (2016). Vaccine protection
1014 against Zika virus from Brazil. Nature *536*, 474–478.

1015 Lazear, H.M., Govero, J., Smith, A.M., Platt, D.J., Fernandez, E., Miner, J.J., and Diamond,
1016 M.S. (2016). A Mouse Model of Zika Virus Pathogenesis. Cell Host Microbe *19*, 720–730.

1017 Lessler, J., Ott, C.T., Carcelen, A.C., Konikoff, J.M., Williamson, J., Bi, Q., Kucirka, L.M.,
1018 Cummings, D.A.T., Reich, N.G., and Chaisson, L.H. (2016). Times to key events in Zika virus
1019 infection and implications for blood donation: A systematic review. Bull. World Health Organ. *94*,
1020 841–849.

1021 Liao, H.-X., Levesque, M.C., Nagel, A., Dixon, A., Zhang, R., Walter, E., Parks, R., Whitesides,
1022 J., Marshall, D.J., Hwang, K.-K., et al. (2009). High-throughput isolation of immunoglobulin
1023 genes from single human B cells and expression as monoclonal antibodies. J Virol Methods
1024 *158*, 171–179.

1025 Lima, J., Martins, C., Leandro, M.J., Nunes, G., Sousa, M.J., Branco, J.C., and Borrego, L.M.
1026 (2016). Characterization of B cells in healthy pregnant women from late pregnancy to post-
1027 partum: A prospective observational study. BMC Pregnancy Childbirth *16*, 139.

1028 Lobo, E.D., Hansen, R.J., and Balthasar, J.P. (2004). Antibody pharmacokinetics and
1029 pharmacodynamics. J. Pharm. Sci. *93*, 2645–2668.

1030 Long, F., Doyle, M., Fernandez, E., Miller, A.S., Klose, T., Sevvana, M., Bryan, A., Davidson, E.,
1031 Doranz, B.J., Kuhn, R.J., et al. (2019). Structural basis of a potent human monoclonal antibody
1032 against Zika virus targeting a quaternary epitope. Proc. Natl. Acad. Sci. U. S. A. *116*, 1591–
1033 1596.

1034 Maciejewski, S., Ruckwardt, T.J., Morabito, K.M., Foreman, B.M., Burgomaster, K.E., Gordon,
1035 D.N., Pelc, R.S., DeMaso, C.R., Ko, S.Y., Fisher, B.E., et al. (2020). Distinct neutralizing
1036 antibody correlates of protection among related Zika virus vaccines identify a role for antibody
1037 quality. Sci. Transl. Med. *12*, 9066.

1038 Malafa, S., Medits, I., Aberle, J.H., Aberle, S.W., Haslwanter, D., Tsouchnikas, G., Wölfel, S.,
1039 Huber, K.L., Percivalle, E., Cherpillod, P., et al. (2020). Impact of flavivirus vaccine-induced
1040 immunity on primary Zika virus antibody response in humans. PLoS Negl. Trop. Dis. *14*,
1041 e0008034.

1042 Mason, R.A., Tauraso, N.M., Spertzel, R.O., and Ginn, R.K. (1973). Yellow fever vaccine: direct
1043 challenge of monkeys given graded doses of 17D vaccine. Appl. Microbiol. *25*, 539–544.

1044 Mehlhop, E., Nelson, S., Jost, C.A., Gorlatov, S., Johnson, S., Fremont, D.H., Diamond, M.S.,
1045 and Pierson, T.C. (2009). Complement Protein C1q Reduces the Stoichiometric Threshold for
1046 Antibody-Mediated Neutralization of West Nile Virus. Cell Host Microbe *6*, 381–391.

1047 Metz, S.W., Thomas, A., Brackbill, A., Forsberg, J., Miley, M.J., Lopez, C.A., Lazear, H.M., Tian,
1048 S., and de Silva, A.M. (2019). Oligomeric state of the ZIKV E protein defines protective immune
1049 responses. Nat. Commun. *10*, 1–7.

1050 Monath, T. (1971). Neutralizing antibody responses in the major immunoglobulin classes to
1051 Yellow Fever 17D vaccination of humans. Am. J. Epidemiol. *93*, 122–129.

1052 Morabito, K.M., and Graham, B.S. (2017). Zika Virus Vaccine Development. J. Infect. Dis. *216*,
1053 S957–S963.

1054 Mrozek-Gorska, P., Buschle, A., Pich, D., Schwarzmayr, T., Fechtner, R., Scialdone, A., and
1055 Hammerschmidt, W. (2019). Epstein–Barr virus reprograms human B lymphocytes immediately
1056 in the prelatent phase of infection. Proc. Natl. Acad. Sci. *116*, 16046–16055.

1057 Mukherjee, S., Sirohi, D., Dowd, K.A., Chen, Z., Diamond, M.S., Kuhn, R.J., and Pierson, T.C.
1058 (2016). Enhancing dengue virus maturation using a stable furin over-expressing cell line.
1059 Virology *497*, 33–40.

1060 Müller, R., Gräwert, M.A., Kern, T., Madl, T., Peschek, J., Sattler, M., Groll, M., and Buchner, J.
1061 (2013). High-resolution structures of the IgM Fc domains reveal principles of its hexamer
1062 formation. Proc. Natl. Acad. Sci. U. S. A. *110*, 10183–10188.

1063 Nguyen, T.G., Ward, C.M., and Morris, J.M. (2013). To B or not to B cells-mediate a healthy
1064 start to life. Clin. Exp. Immunol. *171*, 124–134.

1065 Nielsen-Saines, K., Brasil, P., Kerin, T., Vasconcelos, Z., Gabaglia, C.R., Damasceno, L., Pone,
1066 M., Abreu de Carvalho, L.M., Pone, S.M., Zin, A.A., et al. (2019). Delayed childhood
1067 neurodevelopment and neurosensory alterations in the second year of life in a prospective
1068 cohort of ZIKV-exposed children. Nat. Med. *25*, 1213–1217.

1069 Paz-Bailey, G., Rosenberg, E.S., Doyle, K., Munoz-Jordan, J., Santiago, G.A., Klein, L., Perez-
1070 Padilla, J., Medina, F.A., Waterman, S.H., Adams, L.E., et al. (2018). Persistence of Zika Virus
1071 in Body Fluids — Final Report. N. Engl. J. Med. *379*, 1234–1243.

1072   Perkins, S.J., Nealis, A.S., Sutton, B.J., and Feinstein, A. (1991). Solution structure of human
1073   and mouse immunoglobulin M by synchrotron X-ray scattering and molecular graphics
1074   modelling. A possible mechanism for complement activation. J. Mol. Biol. *221*, 1345–1366.

1075   Pettersen, E.F., Goddard, T.D., Huang, C.C., Couch, G.S., Greenblatt, D.M., Meng, E.C., and
1076   Ferrin, T.E. (2004). UCSF Chimera - A visualization system for exploratory research and
1077   analysis. J. Comput. Chem. *25*, 1605–1612.

1078   Premkumar, L., Collins, M., Graham, S., Liou, G.-J.A., Lopez, C.A., Jadi, R., Balmaseda, A.,
1079   Brackbill, J.A., Dietze, R., Camacho, E., et al. (2017). Development of Envelope Protein
1080   Antigens To Serologically Differentiate Zika Virus Infection from Dengue Virus Infection. J. Clin.
1081   Microbiol. *56*.

1082   Ramsland, P.A., Terzyan, S.S., Cloud, G., Bourne, C.R., Farrugia, W., Tribbick, G., Geysen,
1083   H.M., Moomaw, C.R., Slaughter, C.A., and Edmundson, A.B. (2006). Crystal structure of a
1084   glycosylated Fab from an IgM cryoglobulin with properties of a natural proteolytic antibody.
1085   Biochem. J. *395*, 473–481.

1086   Rasche, L., Duell, J., Castro, I.C., Dubljevic, V., Chatterjee, M., Knop, S., Hensel, F.,
1087   Rosenwald, A., Einsele, H., Topp, M.S., et al. (2015). GRP78-directed immunotherapy in
1088   relapsed or refractory multiple myeloma - results from a phase 1 trial with the monoclonal
1089   immunoglobulin M antibody PAT-SM6. Haematologica *100*, 377–384.

1090   Ravichandran, S., Hahn, M., Belaunzarán-Zamudio, P.F., Ramos-Castañeda, J., Nájera-
1091   Cancino, G., Caballero-Sosa, S., Navarro-Fuentes, K.R., Ruiz-Palacios, G., Golding, H., Beigel,
1092   J.H., et al. (2019). Differential human antibody repertoires following Zika infection and the
1093   implications for serodiagnostics and disease outcome. Nat. Commun. *10*, 1–14.

1094   Reynolds, M.R., Jones, A.M., Petersen, E.E., Lee, E.H., Rice, M.E., Bingham, A., Ellington,
1095   S.R., Evert, N., Reagan-Steiner, S., Oduyebo, T., et al. (2017). Vital Signs: Update on Zika
1096   Virus–Associated Birth Defects and Evaluation of All U.S. Infants with Congenital Zika Virus
1097   Exposure — U.S. Zika Pregnancy Registry, 2016. MMWR. Morb. Mortal. Wkly. Rep. *66*, 366–
1098   373.

1099   Richner, J.M., Jagger, B.W., Shan, C., Fontes, C.R., Dowd, K.A., Cao, B., Himansu, S., Caine,
1100   E.A., Nunes, B.T.D., Medeiros, D.B.A., et al. (2017). Vaccine Mediated Protection Against Zika
1101   Virus-Induced Congenital Disease. Cell *170*, 273-283.e12.

1102   Robbiani, D.F., Bozzacco, L., Keeffe, J.R., Khouri, R., Olsen, P.C., Gazumyan, A., Schaefer-
1103   Babajew, D., Avila-Rios, S., Nogueira, L., Patel, R., et al. (2017). Recurrent Potent Human
1104   Neutralizing Antibodies to Zika Virus in Brazil and Mexico. Cell *169*, 597-609.e11.

1105   Rogers, T.F., Goodwin, E.C., Briney, B., Sok, D., Beutler, N., Strubel, A., Nedellec, R., Le, K.,
1106   Brown, M.E., Burton, D.R., et al. (2017). Zika virus activates de novo and cross-reactive
1107   memory B cell responses in dengue-experienced donors. Sci. Immunol. *2*.

1108   Rohou, A., and Grigorieff, N. (2015). CTFFIND4: Fast and accurate defocus estimation from
1109   electron micrographs. J. Struct. Biol. *192*, 216–221.

1110   Van Rompay, K.K.A., Coffey, L.L., Kapoor, T., Gazumyan, A., Keesler, R.I., Jurado, A., Peace,
1111   A., Agudelo, M., Watanabe, J., Usachenko, J., et al. (2020). A combination of two human
1112   monoclonal antibodies limits fetal damage by Zika virus in macaques. Proc. Natl. Acad. Sci.
1113   *117*, 202000414.

1114 Rosenthal, P.B., and Henderson, R. (2003). Optimal determination of particle orientation,
1115 absolute hand, and contrast loss in single-particle electron cryomicroscopy. J. Mol. Biol. *333*,
1116 721–745.

1117 Rouvinski, A., Guardado-Calvo, P., Barba-Spaeth, G., Duquerroy, S., Vaney, M.C., Kikuti, C.M.,
1118 Navarro Sanchez, M.E., Dejnirattisai, W., Wongwiwat, W., Haouz, A., et al. (2015). Recognition
1119 determinants of broadly neutralizing human antibodies against dengue viruses. Nature *520*,
1120 109–113.

1121 Roy, A., Kucukural, A., and Zhang, Y. (2010). I-TASSER: A unified platform for automated
1122 protein structure and function prediction. Nat. Protoc. *5*, 725–738.

1123 Sapparapu, G., Fernandez, E., Kose, N., Bin Cao, Fox, J.M., Bombardi, R.G., Zhao, H., Nelson,
1124 C.A., Bryan, A.L., Barnes, T., et al. (2016). Neutralizing human antibodies prevent Zika virus
1125 replication and fetal disease in mice. Nature *540*, 443–447.

1126 Scheres, S.H.. (2016). Methods in Enzymology, Vol. 579 (Cambridge, MA: Academic Press).

1127 Scheres, S.H.W., Valle, M., and Carazo, J.M. (2005). Fast maximum-likelihood refinement of
1128 electron microscopy images. Bioinformatics *21*.

1129 Sevvana, M., Long, F., Miller, A.S., Klose, T., Buda, G., Sun, L., Kuhn, R.J., and Rossmann,
1130 M.G. (2018). Refinement and Analysis of the Mature Zika Virus Cryo-EM Structure at 3.1 Å
1131 Resolution. Structure *26*, 1169-1177.e3.

1132 Sharp, T.H., Boyle, A.L., Diebolder, C.A., Kros, A., Koster, A.J., and Gros, P. (2019). Insights
1133 into IgM-mediated complement activation based on in situ structures of IgM-C1-C4b. Proc. Natl.
1134 Acad. Sci. U. S. A. *116*, 11900–11905.

1135 Sigworth, F.J. (1998). A maximum-likelihood approach to single-particle image refinement. J.
1136 Struct. Biol. *122*, 328–339.

1137 Sigworth, F.J. (2004). Classical detection theory and the cryo-EM particle selection problem. In
1138 Journal of Structural Biology, (J Struct Biol), pp. 111–122.

1139 Singh, T., Lopez, C.A., Giuberti, C., Dennis, M.L., Itell, H.L., Heimsath, H.J., Webster, H.S.,
1140 Roark, H.K., Merçon de Vargas, P.R., Hall, A., et al. (2019). Efficient transplacental IgG transfer
1141 in women infected with Zika virus during pregnancy. PLoS Negl. Trop. Dis. *13*, e0007648.

1142 Smit, J.M., Moesker, B., Rodenhuis-Zybert, I., and Wilschut, J. (2011). Flavivirus cell entry and
1143 membrane fusion. Viruses *3*, 160–171.

1144 Smith, S.A., de Alwis, A.R., Kose, N., Harris, E., Ibarra, K.D., Kahle, K.M., Pfaf, J.M., Xiang, X.,
1145 Doranz, B.J., de Silva, A.M., et al. (2013). The potent and broadly neutralizing human dengue
1146 virus-specific monoclonal antibody 1C19 reveals a unique cross-reactive epitope on the bc loop
1147 of domain II of the envelope protein. MBio *4*.

1148 Smith, S.A., Silva, L.A., Fox, J.M., Flyak, A.I., Kose, N., Sapparapu, G., Khomandiak, S.,
1149 Ashbrook, A.W., Kahle, K.M., Fong, R.H., et al. (2015). Isolation and characterization of broad
1150 and ultrapotent human monoclonal antibodies with therapeutic activity against chikungunya
1151 virus. Cell Host Microbe *18*, 86–95.

1152 Stettler, K., Beltramello, M., Espinosa, D.A., Graham, V., Cassotta, A., Bianchi, S., Vanzetta, F.,
1153 Minola, A., Jaconi, S., Mele, F., et al. (2016). Specificity, cross-reactivity, and function of
1154 antibodies elicited by Zika virus infection. Science (80-.). *353*, 823–826.

1155 Stone, M., Bakkour, S., Lanteri, M.C., Brambilla, D., Simmons, G., Bruhn, R., Kaidarova, Z.,
1156 Lee, T.H., Orlando Alsina, J., Williamson, P.C., et al. (2020). Zika virus RNA and IgM
1157 persistence in blood compartments and body fluids: a prospective observational study. Lancet
1158 Infect. Dis. *20*, 1446–1456.

1159 Suloway, C., Pulokas, J., Fellmann, D., Cheng, A., Guerra, F., Quispe, J., Stagg, S., Potter,
1160 C.S., and Carragher, B. (2005). Automated molecular microscopy: The new Leginon system. J.
1161 Struct. Biol. *151*, 41–60.

1162 Swanstrom, J.A., Plante, J.A., Plante, K.S., Young, E.F., McGowan, E., Gallichotte, E.N.,
1163 Widman, D.G., Heise, M.T., de Silva, A.M., and Baric, R.S. (2016). Dengue virus envelope
1164 dimer epitope monoclonal antibodies isolated from dengue patients are protective against zika
1165 virus. MBio *7*.

1166 Taylor, H.P., and Dimmock, N.J. (1985). Mechanisms of Neutralization of Influenza Virus by
1167 IgM. J. Gen. Virol *66*, 903–907.

1168 Tonnerre, P., Melgaço, J.G., Torres-Cornejo, A., Pinto, M.A., Yue, C., Blümel, J., de Sousa,
1169 P.S.F., de Mello, V. da M., Moran, J., de Filippis, A.M.B., et al. (2020). Evolution of the innate
1170 and adaptive immune response in women with acute Zika virus infection. Nat. Microbiol. *5*, 76–
1171 83.

1172 Wang, J., Bardelli, M., Espinosa, D.A., Pedotti, M., Ng, T.S., Bianchi, S., Simonelli, L., Lim,
1173 E.X.Y., Foglierini, M., Zatta, F., et al. (2017). A Human Bi-specific Antibody against Zika Virus
1174 with High Therapeutic Potential. Cell *171*, 229-241.e15.

1175 Wec, A.Z., Haslwanter, D., Abdiche, Y.N., Shehata, L., Pedreño-Lopez, N., Moyer, C.L.,
1176 Bornholdt, Z.A., Lilov, A., Nett, J.H., Jangra, R.K., et al. (2020). Longitudinal dynamics of the
1177 human B cell response to the yellow fever 17D vaccine. Proc. Natl. Acad. Sci. U. S. A. *117*,
1178 6675–6685.

1179 Wiersma, E.J., Collins, C., Fazel, S., and Shulman, M.J. (1998). Structural and functional
1180 analysis of J chain-deficient IgM. J. Immunol. *160*, 5979–5989.

1181 Xiao, C., and Rossmann, M.G. (2007). Interpretation of electron density with stereographic
1182 roadmap projections. J. Struct. Biol. *158*, 182–187.

1183 Yaari, G., Vander Heiden, J., Uduman, M., Gadala-Maria, D., Gupta, N., Stern, J.N.H.,
1184 O'Connor, K., Hafler, D., Laserson, U., Vigneault, F., et al. (2013). Models of Somatic
1185 Hypermutation Targeting and Substitution Based on Synonymous Mutations from High-
1186 Throughput Immunoglobulin Sequencing Data. Front. Immunol. *0*, 358.

1187 Yang, J., Yan, R., Roy, A., Xu, D., Poisson, J., and Zhang, Y. (2014). The I-TASSER suite:
1188 Protein structure and function prediction. Nat. Methods *12*, 7–8.

1189 Zhang, Y. (2008). I-TASSER server for protein 3D structure prediction. BMC Bioinformatics *9*.

1190 Zhang, S.L.X., Tan, H.C., Hanson, B.J., and Ooi, E.E. (2010). A simple method for Alexa Fluor
1191 dye labelling of dengue virus. J. Virol. Methods *167*, 172–177.

1192 Zhang, X., Sheng, J., Austin, S.K., Hoornweg, T.E., Smit, J.M., Kuhn, R.J., Diamond, M.S., and
1193 Rossmann, M.G. (2015). Structure of Acidic pH Dengue Virus Showing the Fusogenic
1194 Glycoprotein Trimers. J. Virol. *89*, 743–750.

1195 Zhao, H., Fernandez, E., Dowd, K.A., Speer, S.D., Platt, D.J., Gorman, M.J., Govero, J.,

1196   Nelson, C.A., Pierson, T.C., Diamond, M.S., et al. (2016). Structural Basis of Zika Virus-Specific
1197   Antibody Protection. Cell *166*, 1016–1027.

1198   Zheng, S.Q., Palovcak, E., Armache, J.P., Verba, K.A., Cheng, Y., and Agard, D.A. (2017).
1199   MotionCor2: Anisotropic correction of beam-induced motion for improved cryo-electron
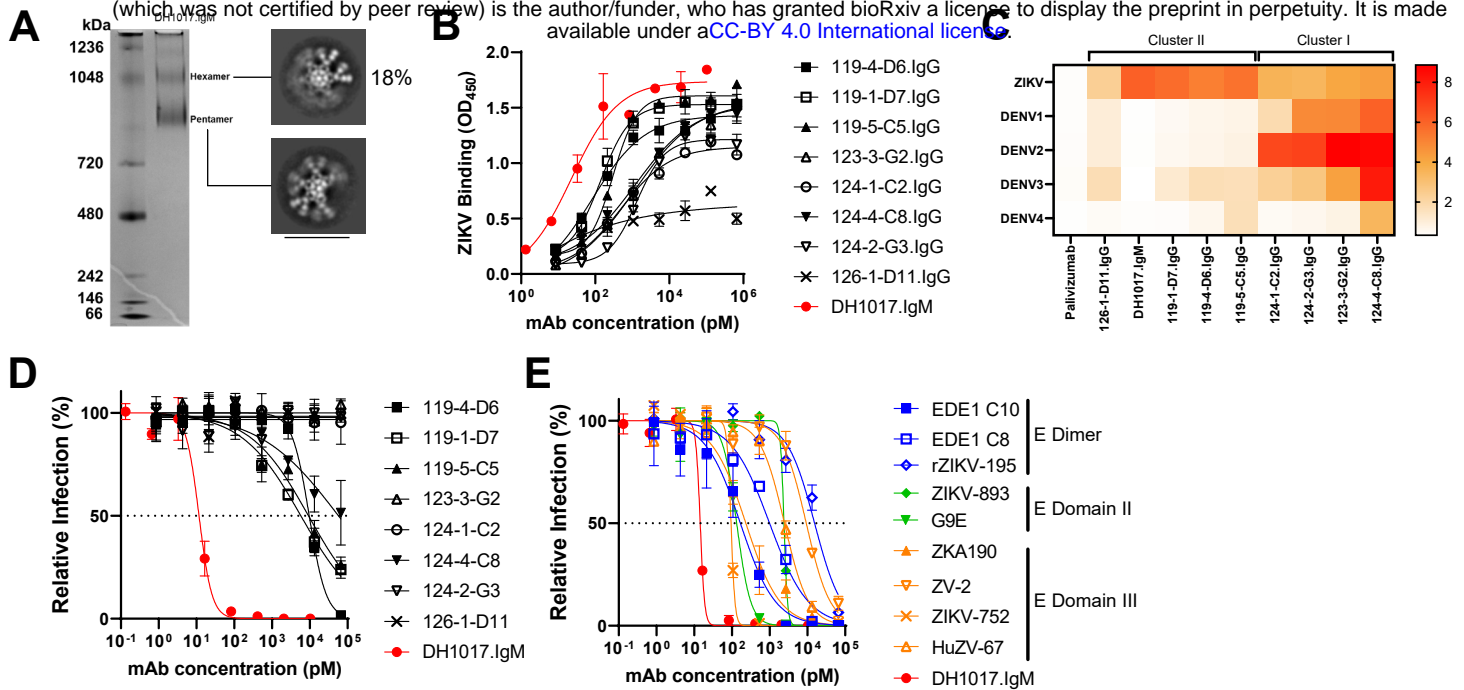1200   microscopy. Nat. Methods *14*, 331–332.

1201

Table 1. Immunogenetics of monoclonal antibodies isolated from B-LCLs. See also **Figure S1** and **Table S2.**
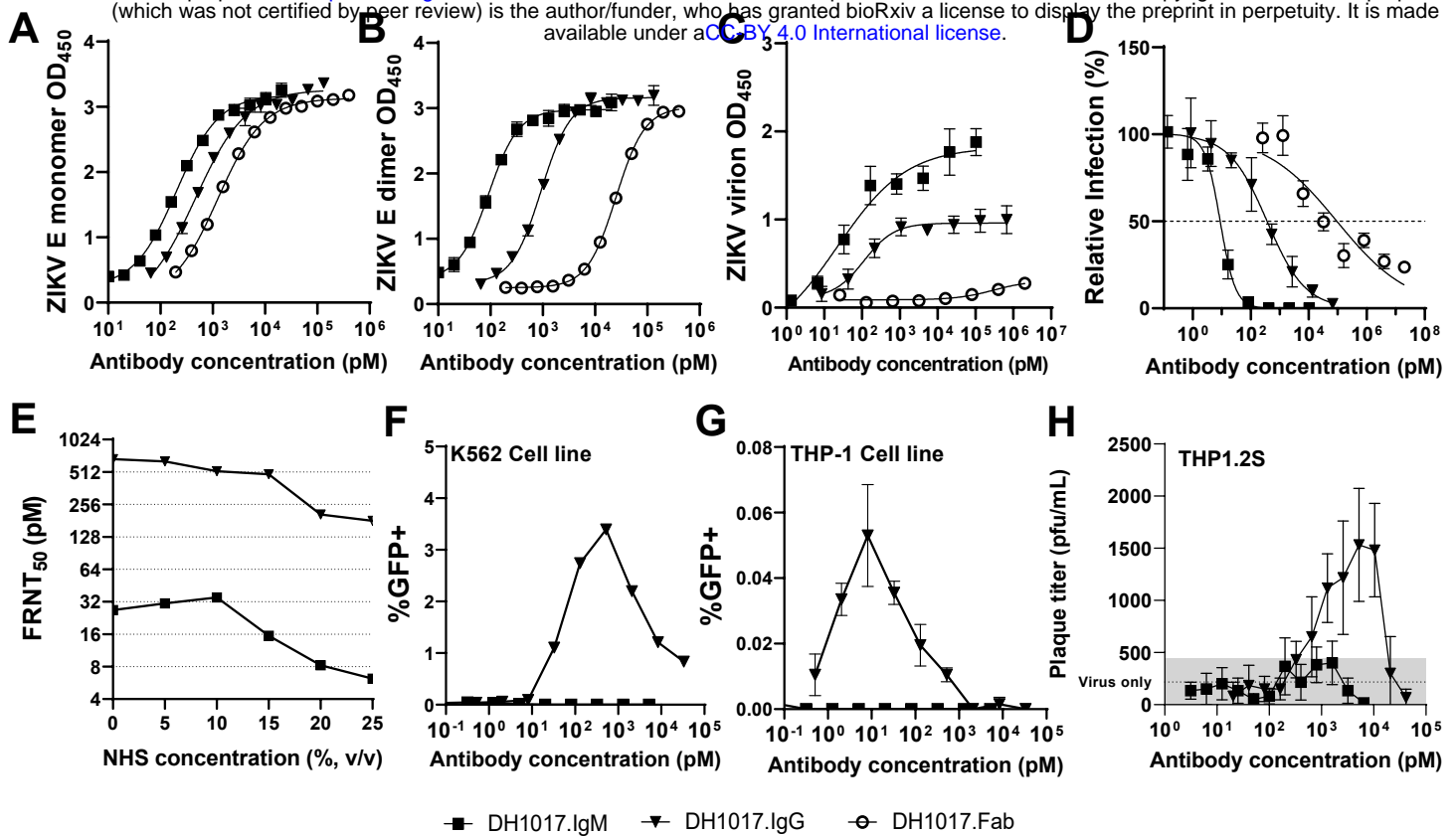
Antibody ID	Source*	V_H	D	J_H	V_H mutation frequency (%)	CDRH3 length (aa)	Isotype	k/l	V_L	J_L	V_L mutation frequency (%)	CDRL3 length (aa)
DH1017.IgM	UBC	4-31	7-27	3	3.8	15	M	lambda	1-51	2	3.37	11
119-4-D6.IgG	UBC	3-64	2-2	6	9.4	13	G1	lambda	3-21	1	7.97	11
119-1-D7.IgG	UBC	3-21	2-15	3	8.4	17	G1	kappa	3-20	2	6.74	10
119-5-C5.IgG	UBC	3-21	6-13	6	3.1	22	G1	kappa	3-11	4	1.52	9
123-3-G2.IgG	MBC	3-30-3	3-3	4	3.1	12	G1	kappa	2-30	4	3.6	9
124-4-C8.IgG	MBC	3-30	3-16	6	9.3	22	G1	kappa	2-28	4	3.0	10
124-1-C2.IgG	MBC	4-39	1-26	4	7.2	15	G1	lambda	2-14	3	5.2	10
124-2-G3.IgG	MBC	3-23	3-10	4	10.8	12	G1	kappa	2-30	1	5.4	8
126-1-D11.IgG	MBC	3-48	4-17	6	4.5	16	G1	kappa	1-39	2	3.8	9

* UBC: unfractionated B cells; MBC: memory B cells
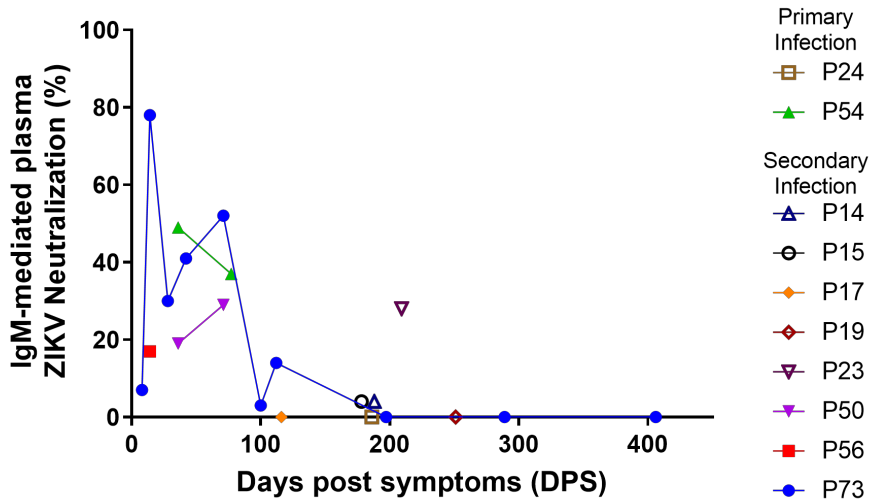
Figure 1. Contribution of plasma IgM to ZIKV neutralization from acute infection through late convalescence. Percent ZIKV neutralization attributable to plasma IgM across ZIKV-infected mothers (n=10) from 8 to 406 days post symptoms (DPS). Each sample tested in three technical replicates. See also **Table S1**.

Figure 2. Characterization of B-LCL-derived ZIKV-specific monoclonal antibodies. A. Left: DH1017.IgM native PAGE gel in non-reducing conditions. Bands identified high and low sized molecular species compatible with IgM hexameric and pentameric forms. Ladder on the left. Right: Negative stain electron microscopy of purified DH1017.IgM showing representative class averages of hexameric and pentameric particles. Scale bar is 40nm. **B.** Binding to whole ZIKV PRVABC59 virions by B-LCL-derived mAbs (n=9). DH1017.IgM is shown in red. Error bars indicate standard deviation of two technical replicates. Experiments were independently repeated twice. **C.** Heatmap showing binding, expressed as LogAUC, to ZIKV and DENV1-4 by the nine B-LCL-derived mAbs. Palivizumab is shown as negative control. Clustering was performed using the Los Alamos Database heatmap tool. **D.** ZIKV PRVABC59 strain neutralization curves of the 9 B-LCL-derived mAbs expressed as percentage of the number of foci relative to the virus alone condition. Dotted line represents 50% viral inhibition. DH1017.IgM is shown in the red filled circle. Error bars indicate standard deviation of assays run in triplicate. Experiments were independently repeated twice. **E.** ZIKV PRVABC59 strain neutralization curves of DH1017.IgM (red) and 9 previously described IgG ZIKV neutralizing antibodies. Colors indicate groups of similar epitopes. Error bars show standard deviation in triplicate measurements. Experiments were independently repeated twice. See also **Figure S2**.

Figure 3. Functional characterization of DH1017.IgM, DH1017.IgG, and DH1017.Fab. A, B. Binding of DH1017.IgM (square), DH1017.IgG (triangle) and DH1017.Fab (circle) mAbs to ZIKV E monomer (A) and dimer (B) measured by ELISA and expressed as optical density at 450nm (OD_{450}). Error bars indicate standard deviation of duplicate observations. Experiments were independently repeated twice. **C.** Whole ZIKV virion binding curves of DH1017.IgM, DH1017.IgG, and DH1017.Fab. Error bars show the standard deviation of two experiments, each run with 6-replicates for DH1017.IgM and DH1017.IgG. DH1017.Fab was run in duplicate. **D.** ZIKV neutralization of serially diluted mAbs. Dotted line denotes 50% relative infection of mAb condition as compared to virus alone ($FRNT_{50}$). Error bars indicate standard deviation of mAbs run in triplicate. Experiments were independently repeated twice. **E.** ZIKV neutralizing titers at 50% viral inhibition ($FRNT_{50}$) over increasing complement concentrations. Normal human serum (NHS) was used as source of complement at the indicated concentrations (v/v). Percent infection of the antibody were calculated relative to the virus alone with matched concentrations of NHS. MAbs were run in triplicate. **F, G**. Serially diluted mAbs were incubated with ZIKV H/PF/2013 reporter virus particles and used to infect K562 (**F**) or THP-1 (**G**) cells to measure antibody-dependent enhancement (ADE) of infection. Enhancement of infection was scored by GFP expression and measured after 36-48 hours using flow cytometry. Representative ADE data of at least three independent experiments are shown. **H.** ADE of DH1017.IgM and DH1017.IgG on THP1.2S cells measured by plaque assay. Dotted line shows mean of six virus-only control replicates and the grey area indicates one standard deviation above and below this mean. Representative results from duplicated experiments run with 6-replicates each. Bars show the standard deviation from 6 replicates. See also **Figure S3**.
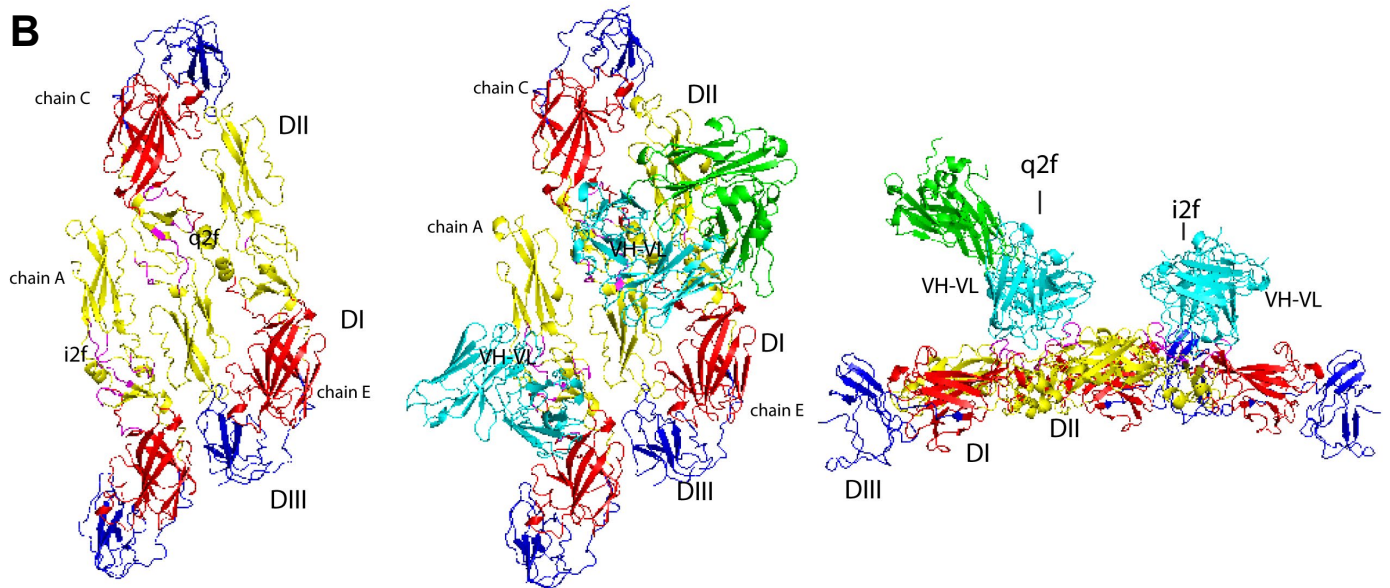
A

Å

C

Å

210.00   240.00

B

D.
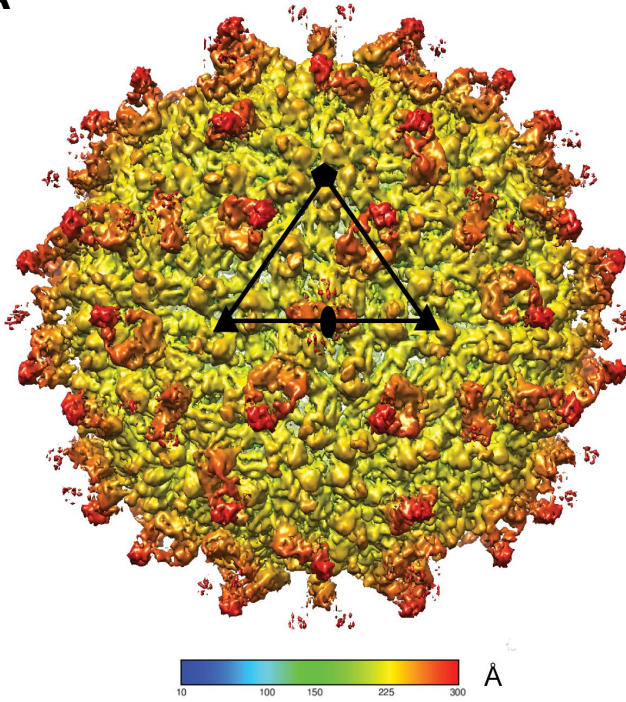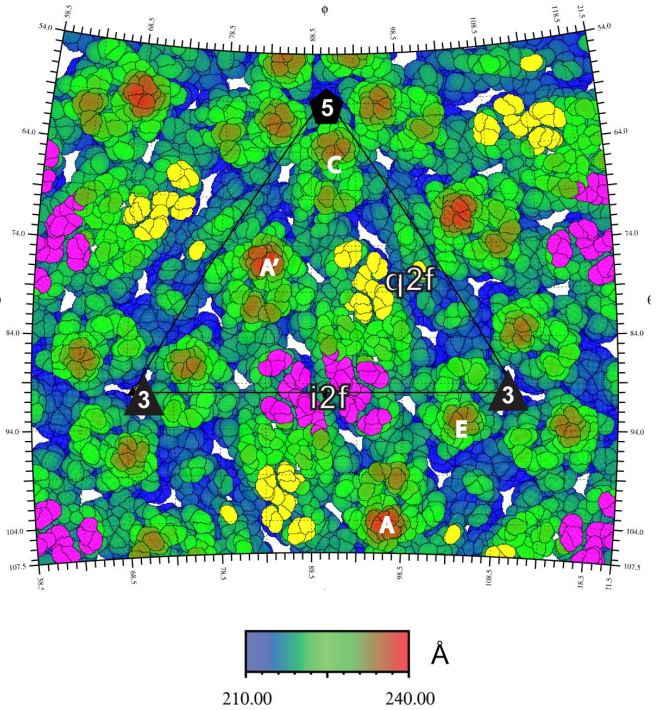
```
IRCIGVSNRD FVEGMSGGTW VDVVLEHGGC VTVMAQDKPT VDIELVTTTV SNMAEVRSYC YEASISDMAS DSRCPTQGEA YLDKQSDTQY VCKRTLVDRG 100
WGNGCGLFGK GSLVTCAKFA CSKKMTGKSI QPENLEYRIM LSVHGSQHSG MIVNDTGHET DENRAKVEIT PNSPRAEATL GGFGSLGLDC EPRTGLDFSD 200
LYYLTMNNKH WLVHKEWFHD IPLPWHAGAD TGTPHWNNKE ALVEFKDAHA KRQTVVVLGS QEGAVHTALA GALEAEMDGA KGRLSSGHLK CRLKMDKLRL 300
KGVSYSLCTA AFTFTKIPAE TLHGTVTVEV QYAGTDGPCK VPAQMAVDMQ TLTPVGRLIT ANPVITESTE NSKMMLELDP PFGDSYIVIG VG 392
```

Figure 4. DH1017 clone interacts with envelope dimer. A. Surface-shaded view of the Zika virion bound with the DH1017 Fab fragment at a resolution of 5.3 Å acquired via cryo-EM. The color represents the distance to the center and shown by the colored scale bar in Å. The black triangle represents the asymmetric unit, a pentagon represents the five-fold axis, the triangle the three-fold axis, and the oval the two-fold axis. **B.** Surface representation of the E ectodomain of Zika virus asymmetric unit (PDB 6CO8) shown in top view unbound, then bound with the variable domain of DH1017.Fab (cyan) and the constant domain (green), and a side view of the asymmetric ectodomain bound the DH1017 Fab fragment (left to right). The E ectodomains are colored with DI in red, DII in yellow, and DIII in blue. The residues of the footprint are colored, magenta. See also **Fig. S4 and Table S3**. **C**. A radially colored roadmap (scale bar in Å). The icosahedral and quasi two-fold axes are labelled i2f and q2f, respectively. The monomer chains of two E dimers are labeled A' and A at the i2f, and chains C and E at the q2f. Residues on the surface of the virus within 6 Å of the variable domain structure fit to the density map are colored yellow and magenta. Yellow residues are on chain C at the q2f axis and magenta residues are at the i2f axis on chain A' and A. **D**. Fab DH1017 epitope shown on the primary sequence of E ectodomain. The epitope residues are colored magenta and the domains DI, DII, and DIII are indicated by line color red, yellow and blue, respectively.
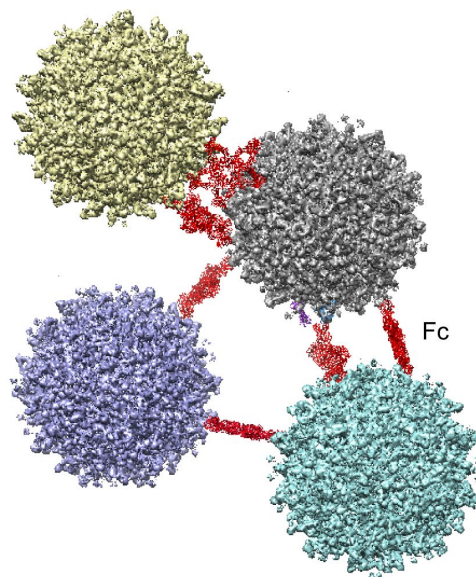
A

B Top down views of virus in icosahedral cage

i2f axis   i5f axis   i3f axis

C
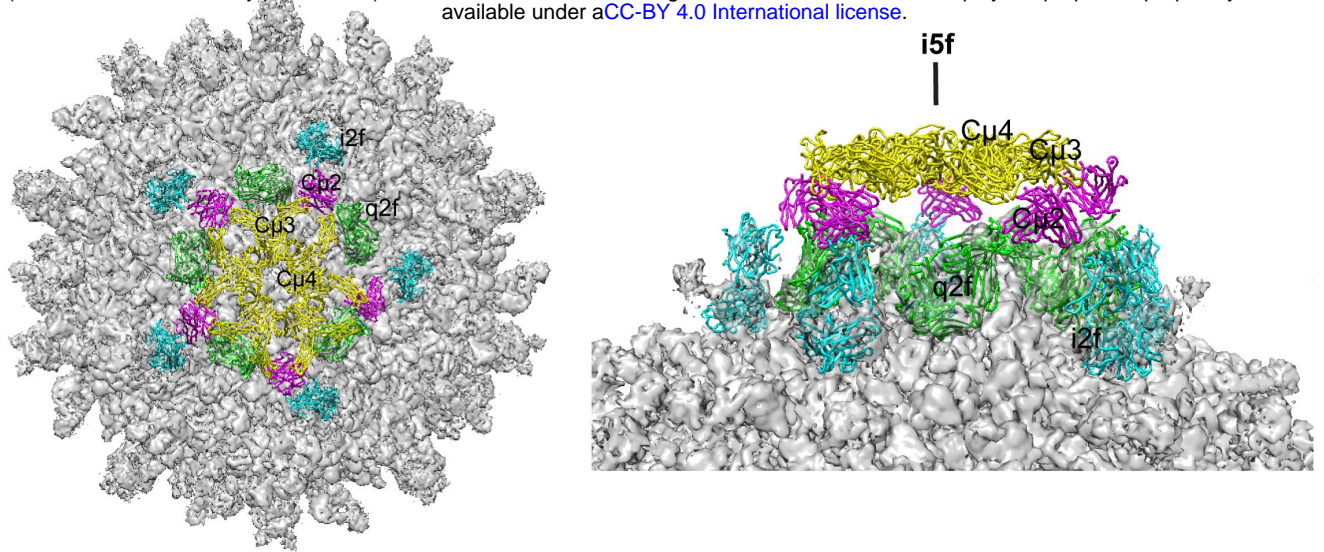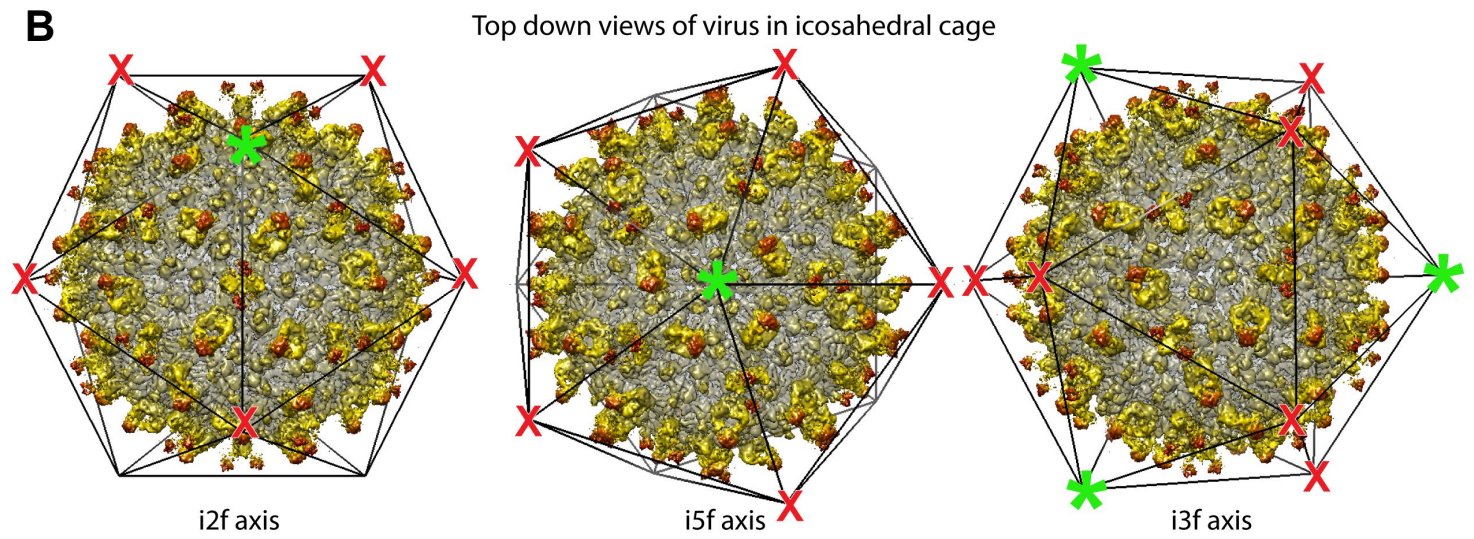
Fc

Figure 5: Models of IgM pentamer bound to Zika virus particle. A. A top down and side view of a model of the pentamer binding the Zika virus particle in an umbrella like conformation. The density map is shown in gray. The Fc domain is shown in yellow, domains Cμ3 and Cμ4 are labeled. The Cμ2 domain is labeled and colored purple. The DH1017 Fab structure is fit to the density map, at the i2f it is cyan and at the q2f, green. **B.** The density map of the Fab bound virus particle in an icosahedral cage with top-down views at each icosahedral axis, i2f, i5f, and i3f. The green asterisk indicates a position where the pentamer is bound as in A. The red X indicates the position of five-fold axes related to the green asterisk by two-fold symmetry that do not have the i2f position available for Fab binding to form the umbrella like conformation. The i3f view shows positions of complete occupancy for the particle bound as in A. **C.** Schematic representation of virus particles crosslinked by pentamers. The Fc portion of the molecule is shown in red crosslinking virus.
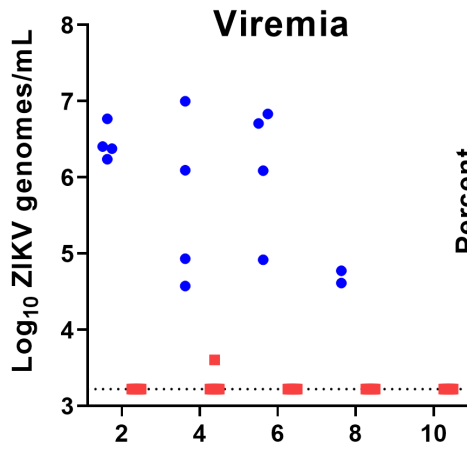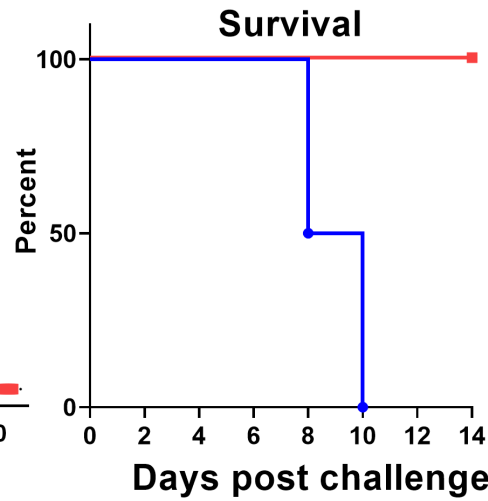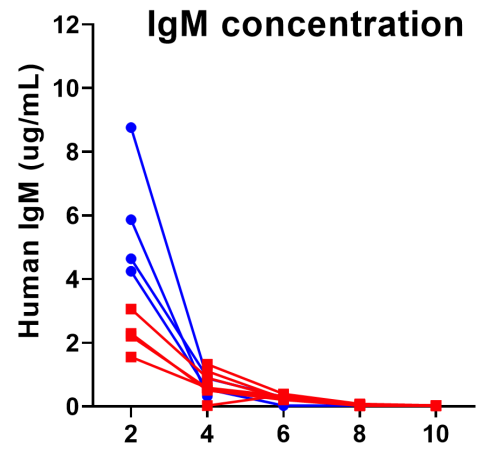
Figure 6: DH1017.IgM protects mice against lethal ZIKV challenge. Five-week-old *Ifnar1*^{-/-} mice were challenged with 1000 focus forming units (FFU) of ZIKV H/PF/2013 in the footpad on day 0. At 1 day prior, and 1 day post challenge, mice were intravenously administered 100μg of human IgM monoclonal antibody, either DH1017.IgM (n=7) or ZIKV non-binding IgM (n=4). Sera was sampled serially up to 14 days post challenge. **A.** Viral load in serum was assessed by qRT-PCR and limit of detection was 1000 copies/mL. **B.** Survival curves for each IgM intervention group. **C.** Total human IgM concentrations were measured in mouse sera by ELISA over days post challenge. Limit of detection for this assay was 0.08-0.03 μg/mL across assays.